

Identifying states of collateral sensitivity during the evolution of therapeutic resistance in Ewing's sarcoma

Jessica A. Scarborough^{1,2}, Erin McClure^{1,3}, Peter Anderson⁴, Andrew Dhawan⁵, Arda Durmaz^{1,2}, Stephen L. Lessnick^{6,7}, Masahiro Hitomi¹, and Jacob G. Scott^{1,2,8*}

¹Translational Hematology and Oncology Research, Taussig Cancer Institute, Cleveland Clinic, Cleveland, OH

²Systems Biology and Bioinformatics Department, School of Medicine, Case Western Reserve University, Cleveland, OH

³Morsani College of Medicine, University of South Florida, Tampa, FL

⁴Heme/Onc/BMT, Cleveland Clinic, Cleveland, OH

⁵Neurological Institute, Cleveland Clinic, Cleveland, OH

⁶Center for Childhood Cancer and Blood Diseases, Abigail Wexner Research Institute at Nationwide Children's Hospital, Columbus, OH

⁷Division of Pediatric Heme/Onc/BMT, The Ohio State University, Columbus, OH

⁸Department of Radiation Oncology, Cleveland Clinic, Cleveland, OH

*scottj10@ccf.org

ABSTRACT

Ewing's sarcoma (EWS) is the second most common primary malignant bone cancer in children. Advances in the treatment of EWS are desperately needed, particularly in the case of metastatic disease. A deeper understanding of collateral sensitivity, where the evolution of therapeutic resistance to one drug aligns with sensitivity to another drug, may improve our ability to effectively target this disease. For the first time in a solid tumor, we examine the repeatability of collateral sensitivity in EWS cell lines over time as evolutionary replicates evolve resistance to standard treatment. In doing so, we produced a temporal collateral sensitivity map that allows us to examine the evolution of collateral sensitivity and resistance in EWS. We found that the evolution of collateral sensitivity and resistance was predictable with some drugs, but had significant variation in response to other drugs. Samples that were most sensitive and most resistant to all drugs were compared using differential gene expression. Using this map of temporal collateral sensitivity in EWS, we can see that the path towards collateral sensitivity is not always repeatable, nor is there always a clear trajectory towards resistance or sensitivity. Identifying transcriptomic changes that accompany these states of transient collateral sensitivity could improve treatment planning for EWS patients.

1 Introduction

2 Ewing's sarcoma (EWS) is the second most common primary malignant bone cancer in children.^{1,2} Localized disease has a
3 50-70% 5-year survival rate, and metastatic disease has a devastating 18-30% 5-year survival rate.²⁻⁴ Advances in the treatment
4 of EWS are desperately needed, particularly in the case of metastatic disease. Unfortunately, all recent attempts to improve
5 the chemotherapy regimen for EWS have only yielded modest results for non-metastatic cancer with little-to-no impact on
6 the course of metastatic disease.^{3,5} Researchers have tried adding ifosfamide and etoposide to standard EWS chemotherapy,
7 increasing the drug doses administered, and decreasing the interval between doses, all without meaningful improvement to
8 metastatic disease outcomes.^{3,5,6} Even when treatment is initially successful, EWS often evolves therapeutic resistance, which
9 ultimately leads to disease relapse.⁷ A deeper understanding of the evolutionary dynamics at play as EWS develops therapeutic
10 resistance may improve our ability to effectively target this disease.

11 During the evolution of therapeutic resistance, both bacteria and cancer can exhibit a phenomenon termed collateral
12 sensitivity, where resistance to one drug aligns with sensitivity to another drug.⁸⁻¹⁰ Likewise, collateral resistance occurs when
13 resistance to one drug aligns with resistance to another drug. The relationship between genotype (e.g. gene expression, somatic
14 mutations, etc.) and fitness of a cell line can be represented by a fitness landscape. In the case of drug response, we define
15 fitness as the EC50 of a cell line to a given drug, where increasing EC50 denotes higher fitness in the presence of this drug. Of
16 importance, a cell line with the same genotype may have varying fitnesses (EC50s) under the selection pressure of different
17 drugs.

18 In collateral resistance, the fitness landscapes of the organism (bacteria or cancer) in the presence of each drug would show

“positive correlation.”¹¹ This is because genotypic changes that cause increased fitness in presence of the first drug also allow increased fitness in the presence of the second drug as well. Next, comparing fitness landscapes in the setting of collateral sensitivity will show “negative correlation,” where genotypic changes leading to increased fitness in the presence of the first drug will cause decreased fitness in the presence of the second drug. Finally, comparing fitness landscapes in the presence of different treatments will not always demonstrate clear positive or negative correlation. Instead, the evolution of resistance to one drug may lead to variable changes in response to the second drug. In this setting, the evolutionary landscapes would be “uncorrelated.” Here, predictive models would be especially useful in treatment planning, as relative collateral sensitivity or resistance cannot be inferred based solely on treatment history.

In the case of collateral sensitivity, a clinician could ideally control disease progression by switching to a collaterally sensitive drug whenever resistance develops. Even if the illness was never completely eradicated, the pathogen or neoplasm would be dampened enough to minimize harm to the patient. Yet, evolution is rarely so easy to predict. Several studies have aimed to identify examples of collateral sensitivity in either bacteria or cancer, and many have shown that exposure to identical therapies have resulted in different responses between evolutionary replicates.^{11–16} These intermediate steps are crucial for determining whether the evolution of therapeutic resistance leads to a collateral fitness landscape that is consistently positively/negatively correlated or uncorrelated through time. Additionally, Zhao et al., examined changes in collateral sensitivity in acute lymphoblastic leukemia (ALL) over time.¹⁴ Here, they produced temporal collateral sensitivity maps to show how drug response evolved over time and between evolutionary replicates.¹⁴ Although Zhao et al. did examine these changes through time, many collateral sensitivity experiments compare only initial and final drug response after resistance to the primary treatment has evolved.^{11, 15}

Table 1. All drugs referenced in the study, their abbreviations, and classifications.

Drug Name	Abbreviation	Class
Dactinomycin	ActD	Antineoplastic antibiotic
Cyclophosphamide	Cyclo	Alkylating agent
Ifosfamide	Ifo	Alkylating agent
Doxorubicin	Doxo	Anthracycline
Etoposide	Etp	Topoisomerase II inhibitor
Olaparib	Ola	PARP inhibitor
Pazopanib	Paz	Tyrosine kinase inhibitor
Vorinostat	SAHA	Histone deacetylase inhibitor
Irinotecan (active metabolite)	SN38	Topoisomerase I inhibitor
SP-2509	SP	Lysine-specific demethylase 1 inhibitor
Temozolomide	TMZ	Alkylating agent
Vincristine	Vin	Alkaloid
Sodium thiosulfate	NaThio	Drug activation reagent

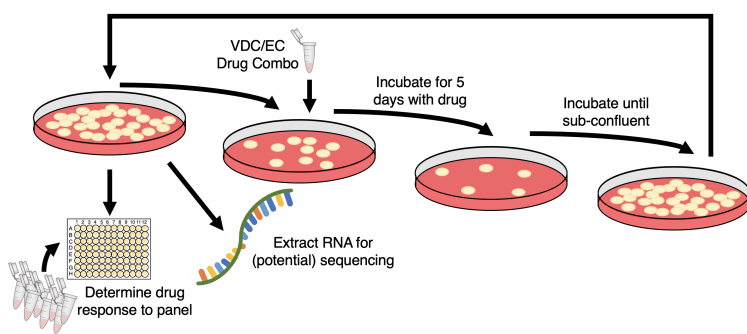


Figure 1. Overview of experimental evolution of resistance in Ewings sarcoma cell lines. As cells recovered from each exposure, cells were tested for their sensitivity for a panel of drugs and samples were frozen for potential use in RNA-sequencing. The drug dosage was only increased once throughout the experiment, at the fifth exposure to the VDC combination, described in Methods. Additionally, drug toxicity assays are performed at each time point to evaluate changes in therapeutic resistance or sensitivity over time. Although each cell line began with 5 experimental and 3 control evolutionary replicates, the A673 cell line lost one experimental replicate due to contamination.

For the first time in a solid tumor, we examine the repeatability of collateral sensitivity across time as cells evolve resistance to standard treatment. In doing so, we use two EWS cell lines, A673 and TTC466. The A673 cell line contains the *t(11;22)* translocation resulting in the *EWSR1/FLI1* gene fusion.^{17, 18} This fusion is the most common genetic aberration found in 90-95% EWS tumors.^{17, 19} On the other hand, the TTC466 cell line has a *t(21;22)* translocation resulting in the EWS-ERG gene fusion, which only occurs only in 5-10% of EWS tumors.^{17, 19} After splitting the cell lines into evolutionary replicates, they were exposed to standard chemotherapy and their response to a panel of drugs was assessed over time. All drugs included in this study may be found in Table 1. We hypothesize that evolutionary replicates of two Ewing’s sarcoma cell lines repeatedly exposed to standard chemotherapy will demonstrate divergent evolutionary paths despite nearly identical experimental conditions and initial genotype. Finding patterns of collateral resistance (positively correlated land-

scapes), sensitivity (negatively correlated landscapes) or variation (uncorrelated landscapes) within these divergent paths may provide useful insight in exploring new treatment options for EWS patients.

Results

The long term evolution of therapeutic resistance

This work examines the evolution of collateral sensitivity and resistance in two EWS cell lines during repeated exposure to a standard chemotherapy regimen over time. At the onset of the experiment, each cell line was split into eight evolutionary replicates, five experimental and three control. Due to contamination, Replicate 2 from the A673 cell line was excluded from the analysis, leaving four experimental and three control replicates in this cell line. Each experimental evolutionary replicate then underwent the same drug cycling, as demonstrated in Figure 1. Briefly, experimental replicates were incubated in cycles of vincristine-doxorubicin-cyclophosphamide (VDC) and etoposide-cyclophosphamide (EC) combinations.³ This procedure models standard-of-care given to EWS patients, which consists of cycles of vincristine-doxorubicin-cyclophosphamide (VDC) and etoposide-ifosfamide (EI) combinations. Because ifosfamide requires metabolic activation and no activated compound is commercially available, we chose to substitute ifosfamide for cyclophosphamide, as these compounds are analogs.²⁰ Control replicates were maintained in only vehicle control. More details can be found in Methods.

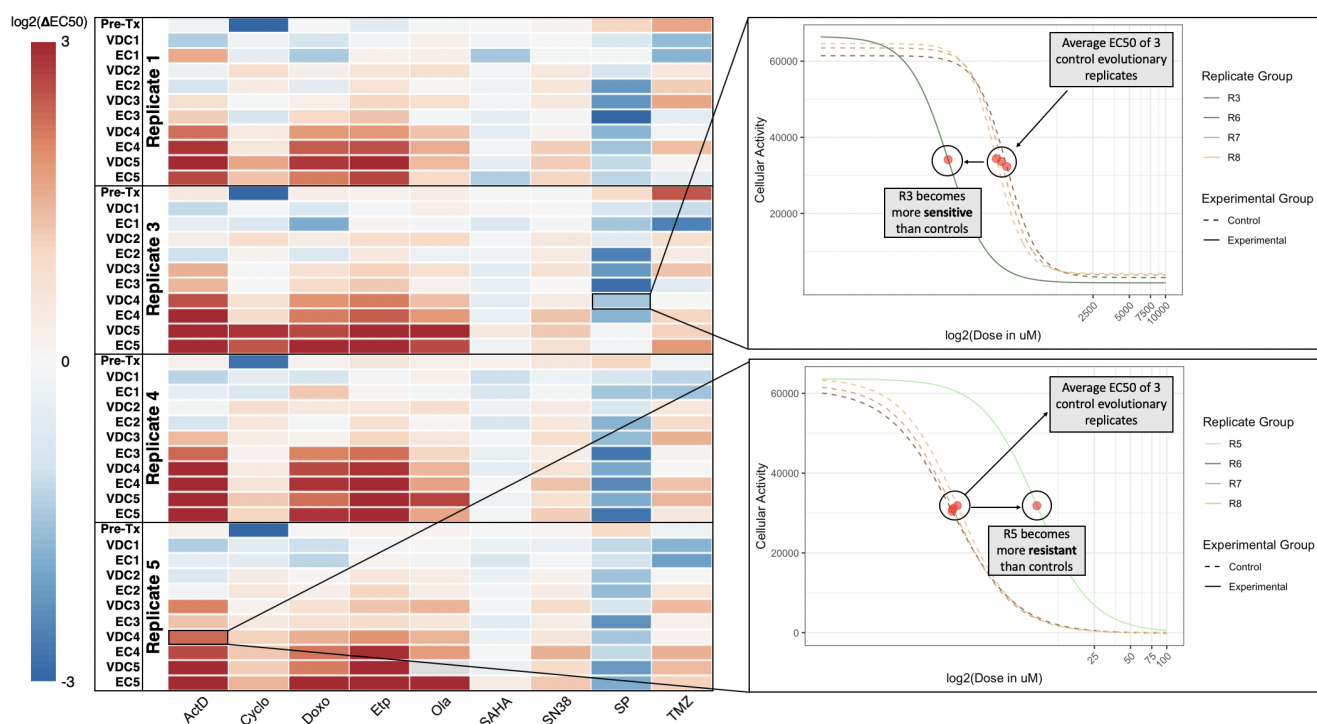


Figure 2. Temporal collateral sensitivity map representing EC50 changes to a panel of drugs as the A673 cell line develops resistance to standard treatment. **Left:** A heatmap representing how the EC50 to a panel of nine drugs changes in 4 A673 cell line evolutionary replicates as they are exposed to the VDC/EC drug combinations over time. Color represents the \log_2 fold change of EC50 to a drug (columns) for a replicate at a given evolutionary time point (rows) compared to the average EC50 of the three control evolutionary replicates at the corresponding time point. Values above $\log_2(3)$ or below $\log_2(-3)$ are represented by $\log_2(3)$ and $\log_2(-3)$, respectively. Time points are denoted as the drug combination that a given replicate has recently recovered from. For example, the data representing dose-response models after the first application of the VDC drug combination would be labeled with VDC1. Of note, the EC50 of olaparib in Replicate 5 at the VDC5 timepoint is indeterminate due to a poorly fit dose-response model. This value in the heatmap is denoted as gray, but Supplementary Figure 1 remains uncensored. **Right:** Top, a plot of the dose-response curves for Replicate 3 and all control replicates (Replicates 6, 7, 8) in response to SP-2509 (SP) at the VDC4 time point. Bottom, a plot of the dose-response curve for Replicate 5 and all control replicates in response to dactinomycin at the VDC4 time point. Cellular activity is measured by enzymatic conversion of alamarBlue, normalized to background fluorescence. Estimated EC50 for each replicate is denoted with a red circle. These two dose-response plots demonstrate how the heatmap (left) values were calculated, where the control EC50 values are averaged and the heatmap values represent the \log_2 fold change between a given replicate and this mean EC50 value.

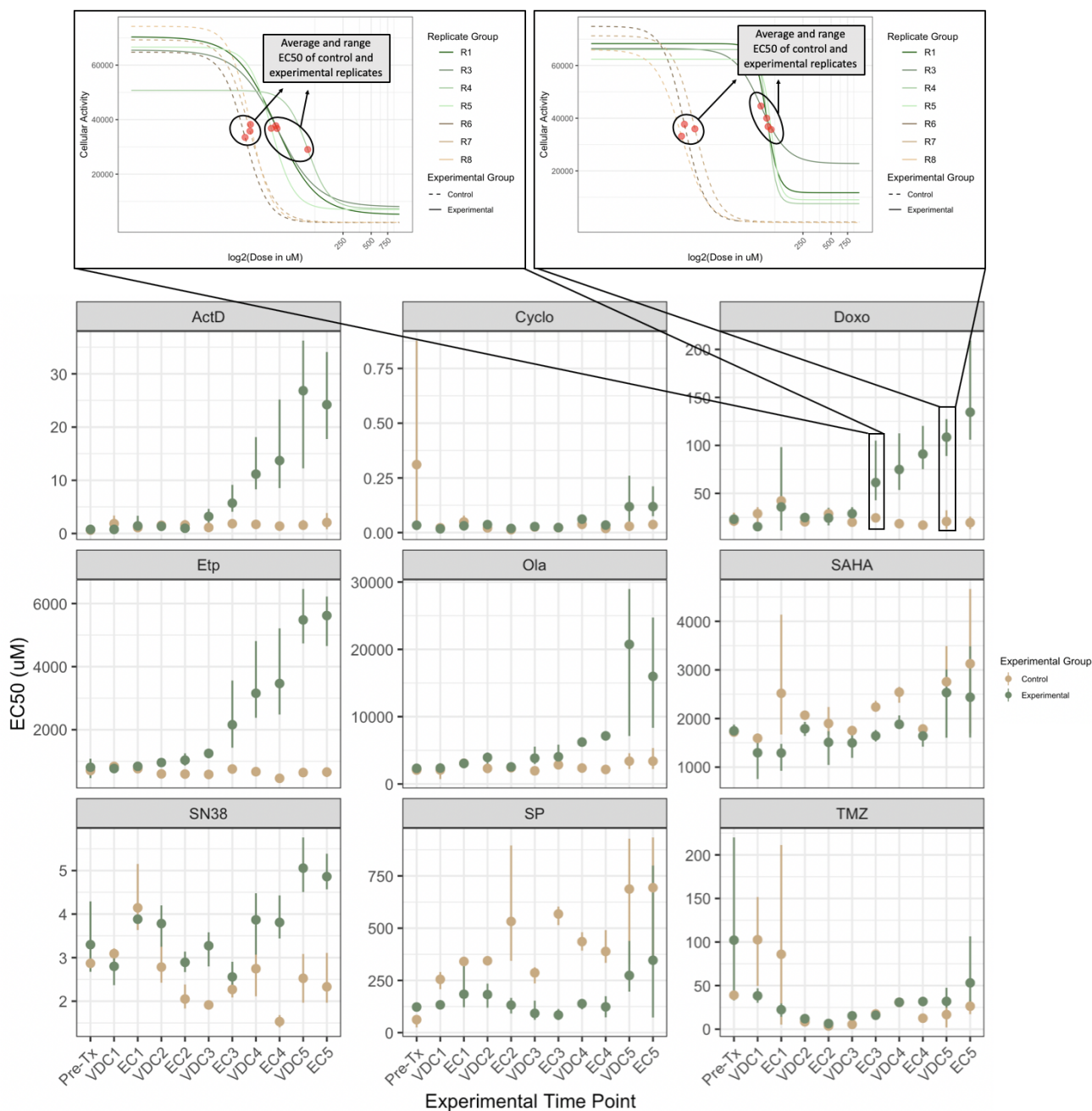


Figure 3. Point-range plots demonstrating EC50 changes in A673 experimental and control replicates over time.

Bottom: Point-range plots representing the changes in drug response to a panel of nine drugs. Experimental time points (x-axis) represent which step in the drug cycle the replicates have just recovered from. Points on the plot represent the average EC50 for the group, either experimental or control. Lines represent the range for the entire group. The EC50 of olaparib for Replicate 5 after the fifth exposure to VDC is indeterminate due to a poorly fit dose-response model, and has been removed from this drug's VDC5 time point experimental group EC50 average and range calculations. This value has not been censored in Supplemental Figures 1 and 2. The y-axis of all the point-range plots has uM units, except Cyclo, where the unit is percent of chemically activated 4-hydroxycyclophosphamide solution by volume. **Top:** Two plots demonstrating a more detailed view of the dose-response data represented at the EC3 and VDC5 time points in the Doxo point-range chart. Cellular activity is measured by enzymatic conversion of alamarBlue, normalized to background fluorescence. Comparing these two plots shows the clear divergence in drug response between experimental and control evolutionary replicates as the treatment regimen continued.

88 After proliferating to sub-confluent density in maintenance medium, a fraction of cells from all evolutionary replicates were
89 snap frozen for RNA extraction, another fraction underwent drug sensitivity assays to 12 drugs, and another fraction of the cells
90 were plated for exposure to the next cycle of the alternate drug combination. For each drug at each time point, the EC50 of
91 each evolutionary replicate was derived by fitting the drug-response triplicate data to a four-parameter log-logistic model as
92 described in Methods. A plot of all dose-response triplicates with their estimated EC50 can be found in the linked GitHub
93 repository.

94 **Discerning changes in chemo-sensitivity and -resistance across time**

95 Figures 2 and 3 display the changes in drug response to 9 agents over time in the A673 cell line. In addition to the nine drugs
96 displayed this figure, two additional drugs (Pazopanib and Vincristine) and a drug activation reagent (sodium thiosulfate) were
97 included in the drug sensitivity assays. Data for these drugs are included in Supplemental Figures 1 and 2. Heatmap and
98 point-range plots for the for the TTC466 cell line can be found in Supplemental Figures 3 and 4, respectively.

99 Figure 2 shows a temporal collateral sensitivity map which represents the log₂ fold change of EC50 to a drug (columns) for
100 an experimental replicate at a given time point (rows) compared to the average EC50 of the three control evolutionary replicates
101 to the same drug, at that time point. The right panel of Figure 2 provides examples of how each heatmap value is calculated.
102 Top, we see the drug response of Replicate 3 to SP-2509 after its fourth exposure to VDC (VDC4), along with the three control
103 evolutionary replicates at this time point. This example demonstrates a move towards sensitivity in the experimental replicate.
104 Below, we can interrogate Replicate 5 at the same time point in response to dactinomycin, where the EC50 of this experimental
105 replicate is more resistant than the control replicates. The temporal collateral sensitivity maps found in Supplementary Figures 1
106 and 3 include the log₂ fold change for the each control evolutionary replicate from the average of the three control evolutionary
107 replicates at the corresponding time point. Ideally, this value will be close to zero (white), because the three control replicates
108 should have similar EC50s.

109 Figure 3 contains point-range plots for the nine drugs included in our analysis demonstrating the average and range of
110 EC50 values for experimental and control replicates at each time point in the experiment. The top panel of Figure 3 uses
111 data from the doxorubicin (Doxo) drug sensitivity assay in the A673 cell line to demonstrate how the point-range plot values
112 were calculated. The average and range of EC50 values are calculated for experimental and control replicates. At each time
113 point, both the experimental and control point-range values are displayed to demonstrate whether they change and/or diverge
114 over time. In response to doxorubicin, the control replicates remained stable across each progressive time point, but the
115 experimental replicates became increasingly more resistant as they were repeatedly exposed to standard treatment. Examining
116 these point-range plots also allows us to observe the overall stability of drug response in control replicates, which are not
117 being evolved under the selection pressure of the VDC/EC drug cycling. For example, the EC50 range for control replicates to
118 dactinomycin is so minimal that the lines representing range are not visible for most time points in the ActD panel of Figure 3.
119 On the other hand, control replicates show significant variation in their response to SN38 and temozolomide (TMZ) at many
120 time points.

121 **Surveying the stochasticity of evolution**

122 While examining Figures 2 and 3, we see predictable development of collateral sensitivity and resistance to some drugs, but
123 evolutionary stochasticity was observed in the response to others. For example, the cells were initially sensitive to dactinomycin
124 and moved into a distinct state of collateral resistance in all replicates. This leads us to the preliminary conclusion that the
125 evolutionary landscape of the cells under the VDC/EC selection pressure and the landscape of the cells under the dactinomycin
126 selection pressure would show strong positive correlation. Next, all replicates acquired relatively consistent resistance to
127 doxorubicin and etoposide over time, which is to be expected, because these two reagents are included in the treatment regimen.
128 Unexpectedly, most replicates acquired only mild resistance to cyclophosphamide, a drug which is included in both cycles of
129 the treatment regimen. All replicates relatively consistently evolved from sensitive to resistant in response to olaparib, SN38,
130 and temozolomide. In response to vorinostat (SAHA), all replicates appear to show minor sensitivity across time, but no
131 discernible trend in toward greater sensitivity nor resistance. Finally, there was moderate sensitivity to SP seen in all A673
132 replicates, again with no discernible trends through time. Due to the variation in response to SAHA or SP over time, we would
133 conclude that the fitness landscapes of cells exposed to these drugs compared to the landscapes of cells exposed to VDC/EC
134 would be relatively uncorrelated.

135 **Differential gene expression analysis provides insight into the mechanisms of drug response**

136 Eighteen samples from the A673 cell line were RNA-sequenced, visualized in the left panel of Figure 4. This cell line was
137 chosen for sequencing because drug sensitivity panels of the controls remained more stable than in the TTC466 cell line. All
138 the samples were ranked based on their response to the 12 drugs included in the drug sensitivity panels. These rankings are
139 visually represented in waterfall plots of the log₂ fold change in EC50 for all sequenced samples against all drugs can be seen
140 in Supplementary Figures 5-16. For each drug, differential gene expression (DE) analysis was performed between samples that

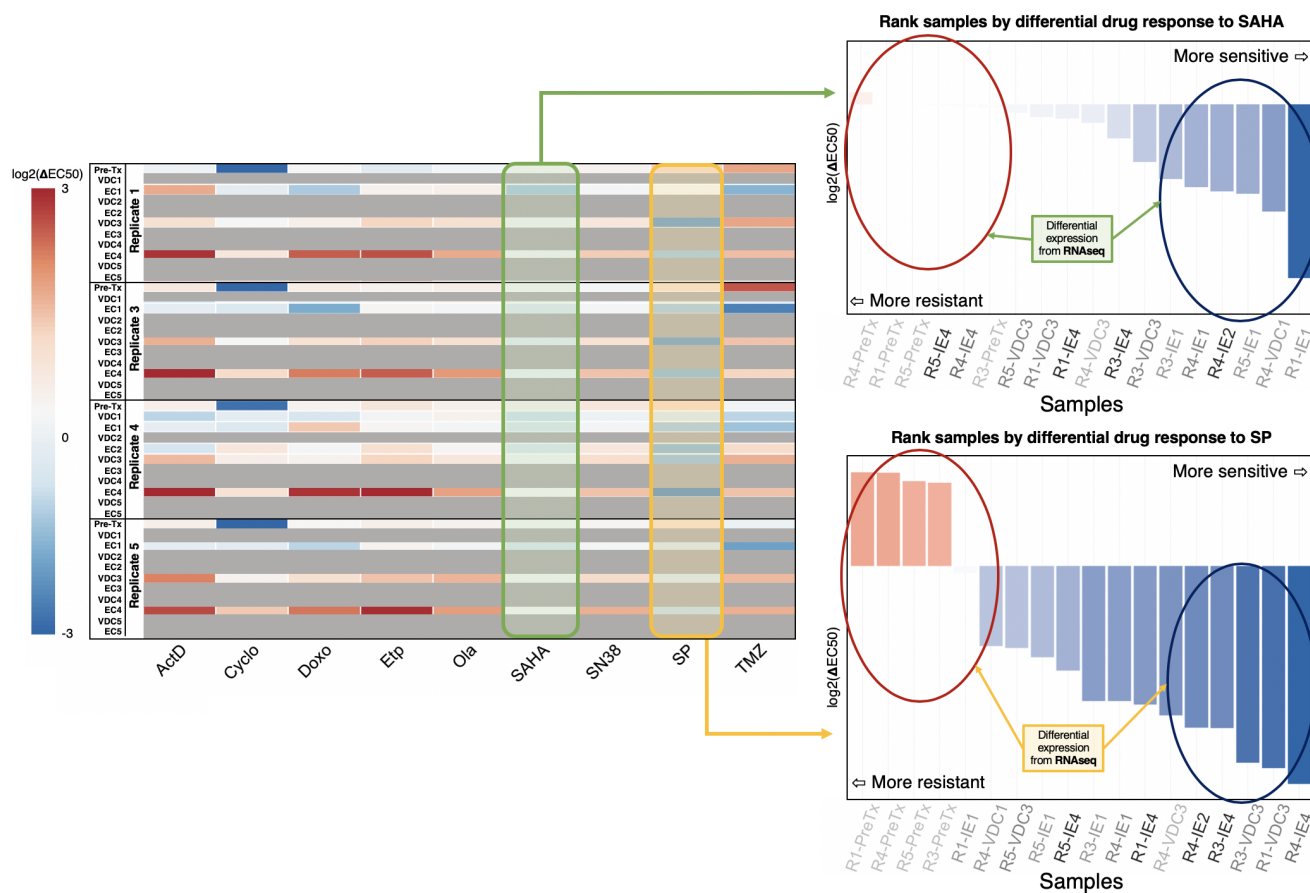


Figure 4. RNA-sequencing and differential gene expression analysis provide insight into states of collateral sensitivity and resistance. Left: The temporal collateral sensitivity map from 2, where all samples that were not sequenced are overlaid with gray. Right: Two waterfall plots representing the samples ranked by their responses to the two drugs, vorinostat (SAHA, top) and SP-2509 (SP, bottom). Sample labels on the x-axis are represented by darker colors the longer they have been evolved in the evolutionary experiment.

Table 2. Genes with significant differential expression between SAHA-resistant and SAHA-sensitive samples. Differential gene expression analysis was performed using EBSseq in R, with maxround set to 15 and FDR of 0.05.

Genes with \uparrow expression in SAHA-sensitive state			
ACOT	ACPP	AHR	B3GNT5
CCL2	FOS	GAL	NUP188
RN7SL5P	SCNN1G	TRAV5	
Genes with \uparrow expression in SAHA-resistant state			
ABCB1	KAZALD1	RPS26	SMAD6
TRGC1			

141 rank in the top and bottom third of responses towards the drug. Results for each drug's DE analyses, including the analyses
 142 highlighted below, may be found in Supplementary Information.

143 In many cases, it is clear that ranking samples by their change in drug response also ranks them based on how long they've
 144 been exposed to the treatment regimen. Although this is not unexpected, interpreting the DE results in this context becomes
 145 more difficult. Significant differences in gene expression may be related to a sample's chemosensitivity/chemoresistance, but

causation cannot be inferred, because these differentially expressed genes may simply be altered in response to continued exposure to the treatment regimen. We chose to highlight the DE analyses where ranking samples in response to a given drug didn't consistently arrange them in the order that they were isolated from the drug-cycling treatment. To that end, the waterfall plots in Supplementary Figures 5-16 have darker sample labels (x-axis) depending on how long they've been exposed to the treatment regimen (e.g. a sample label from the IE2 time point will be lighter than a sample from the IE3 time point). This makes it easier to visualize whether the time points are well distributed in the log₂ fold change rankings.

The right panel of Figure 4 demonstrates how samples were ranked based on their response to vorinostat (SAHA) and SP-2509 (SP). Genes with significantly increased expression in a SAHA-resistant or SAHA-sensitive state are listed in Table 2, while genes with significantly increased expression in an SP-resistant or SP-sensitive state are listed in Table 3.

Table 3. Genes with significant differential expression between SP-resistant and SP-sensitive samples. Differential gene expression analysis was performed using EBSec in R, with maxround set to 15 and FDR of 0.05.

Genes with ↑ expression in SP-sensitive state			
ALX1	AMZ2	APOBEC3C	ARHGEF6
CD63	DCN	FAM72D	FAM92A
HIST1H1T	IL33	IRX3	LINC00326
LITAF	LYN	MRPS18C	NPIPA5
NRG1	PCSK6	PTGR1	PYCARD
RTN	SP100	SSTR1	TMEM192
TSPAN5	YAF2	ZFAND1	ZNF277
Genes with ↑ expression in SP-resistant state			
ADGRL2	ANKS6	AP3B2	AP5Z1
ARHGEF9	C7	CAMKV	CCAR2
CD24	CDH4	CHGA	CORO7
CRMP1	DGCR8	DHCR7	DPP3
EPHA4	FASN	FOXO3B	FRG2FP
GALNS	HBA2	HDAC10	INCENP
INTS1	KSR1	LIN28B	LINC01089
LRCH2	MAN2C1	MEG3	MEG8
MRGPRF	MRNIP	MSRA	NEB
NEFM	NOM1	NUP210	PBX1
PC	PCBP2-OT1	PCDH17	PLXNB1
PPP1R1B	PRRC2B	PTPRG-AS1	PPYGO1
RNF130	RNF44	SBNO2	SCAMP4
SCARA3	SLC16A7	SLC29A2	SLITRK3
SYK	TAF15	TAF1C	TAF6L
TMEM271	TUBB3	VAX1	WDR17
WDR27	ZNF354C	ZNF414	ZNF667
ZNF667-AS1	ZNF675	ZNF730	ZNF736

Discussion

In this work, we evolved two EWS cell lines, A673 and TTC466, with repeated exposure to standard-of-care chemotherapy in order to investigate the evolution of collateral sensitivity and resistance through time. Each cell line was initially split into 8 evolutionary replicates, with 5 experimental replicates exposed to treatment in parallel and 3 control replicates exposed solely to vehicle control. After exposure to each drug cycle, all replicates had cells saved for RNA-sequencing and sensitivity to a panel of 12 drugs was assessed. We produced a temporal collateral sensitivity map to examine the drug sensitivity assays for nine of these drugs through time in the A673 cell line (see Figure 2). Likewise, Figure 3 demonstrates how the average and range EC₅₀ between A673 experimental replicates and control replicates diverged as the experimental replicates continued the drug cycling treatment regimen. Supplementary Figures 1 and 2 contain the drug response changes to all 12 drugs, with no censored data. Supplementary Figures 3 and 4 also exhibit the changes in drug response within the TTC466 cell line; however, the main text focuses on the A673 cell line due to greater observed stability in this cell line's control evolutionary replicates through time.

166 Figure 2 shows that as the A673 experimental replicates were repeatedly exposed to the treatment regimen, states of
167 collateral sensitivity and resistance emerge consistently towards some drugs, while responses to other agents remain variable.
168 For example, despite no exposure to the drug, all replicates consistently moved to a state of collateral resistance towards
169 dactinomycin, providing an example of positively correlated evolutionary landscapes. On the other hand, all replicates show
170 variable collateral sensitivity to SP over time, and there is no clear trend towards a durable state of sensitivity. Similarly, all
171 replicates show variable minimal collateral sensitivity to SAHA, but no state of collateral resistance or sensitivity dominates for
172 many time points or between replicates. Both of these drugs would have uncorrelated evolutionary landscapes in comparison to
173 the landscape under the VDC/EC selection pressure. Additionally, these results imply that although there are consistent changes
174 that allow for collateral resistance to dactinomycin, these changes do not invariably cause a consistent pattern of collateral
175 sensitivity to SAHA or SP. When collateral sensitivity or resistance cannot be consistently identified, gene signatures or other
176 predictive models are especially helpful in treatment planning.

177 Figure 3 also demonstrates these changes in drug sensitivity through time, but it allows for easier interrogation of differences
178 between experimental and replicate groups. Although an increase in EC50 range can be reasonably expected as experimental
179 replicates evolve and diverge under the selective pressure of the VDC/EC regimen, ideally there should be minimal differences
180 in EC50 between control replicates at a given time point. For example, the EC50 range of control replicates in response to
181 dactinomycin over time is so minimal that the point-range plot lines can barely be discerned at any time point. On the other
182 hand, temozolomide shows very significant range in the control replicates in the first few time points.

183 After analyzing the repeatability (or lack thereof) of the evolution of collateral sensitivity and resistance in the A673 EWS
184 cell line, 18 samples from across various time points were sent for RNA-sequencing (Figure 4). We identified significantly
185 increased expression of ABCB1 (also known as MDR1) in the state of SAHA-resistance, seen in Table 2. This gene has
186 previously been implicated in chemotherapeutic multi-drug resistance.²¹ Additionally, CCL2 was found to have increased
187 expression in a SAHA-sensitive state. Using an *in vitro* experiment, Gatti and Sevko et al. describe how adding SAHA to the
188 temozolomide treatment of melanoma may stymie cancer growth by interfering with CCL2 signaling. This is consistent with
189 increased CCL2 expression leading to SAHA sensitivity, as cells that are more reliant on CCL2 signaling could experience a
190 stronger effect from its disruption.²²

191 Next, we see a greater number of differentially expressed genes when examining response to SP than SAHA. SP inhibits
192 lysine-specific demethylase 1 (LSD1, also known as KDMA1), which primarily acts as a histone demethylase.²³ Increased
193 expression of LSD1 has been implicated in many types of cancers (e.g. breast, prostate), and its targeted inhibition is being
194 investigated for therapeutic potential in EWS.²⁴ Due to the novelty of LSD1 inhibitors (including SP-2509), there is very
195 little known regarding genomic biomarkers of sensitivity or resistance. In Table 3, however, we see some notable trends in
196 the significantly differentially expressed genes between good and poor responders to SP. First, many zinc protein fingers,
197 which often play a role in transcriptional regulation, have increased expression in both SP-sensitive and -resistant states.²⁵
198 Additionally, three TATA-box-binding-protein (TBP) associated factor (TAF) proteins have increased expression in SP-resistant
199 states. Again, these genes are implicated in transcriptional regulation.²⁶ Although these results do not imply any one mechanism
200 for SP-sensitivity or -resistance, it is evident that the regulation of gene expression plays a significant role in the response to
201 this drug.

202 As noted previously, states of collateral sensitivity and resistance are often not immutable. Instead, these states are frequently
203 the result of many fleeting evolutionary contingencies. For instance, Nichol et al. demonstrated that after *E. coli* evolved
204 resistance to cefoxatime (a β -lactam antibiotic) in 60 evolutionary replicates, there were highly heterogeneous changes in
205 collateral sensitivity and resistance to alternative antibiotics. Furthermore, this genotypic heterogeneity was discovered as well,
206 with five variants of the β -lactamase gene which likely played a role in the variable drug responses. Additionally, Dhawan et al.
207 derived cell lines of ALK-positive non-small cell lung cancer, where each cell line was resistant to a second-line therapy.¹⁵
208 Subsequently, the cell lines were exposed to the same panel of second-line treatments in an effort to identify drug combinations
209 that elicit collateral sensitivity. The study found that collateral sensitivity was most often evolved towards etoposide and
210 pemetrexed. Although these drugs had the most optimal response, it was inconsistent, leading to the conclusion that collateral
211 sensitivity is a dynamic state, which is a ‘moving target’ instead of a predictable outcome.

212 With this understanding, our experiment would, of course, benefit from even more experimental evolutionary replicates to
213 confirm the repeatability of some observations. For example, the evolution of collateral resistance to dactinomycin in all four
214 A673 experimental replicates is consistently stable in the data presented here. However, given the vast genetic contingencies
215 that lead to changes in drug response, observing said stability over many additional replicates would provide a more convincing
216 argument for the consistent evolution of dactinomycin collateral resistance following exposure to VDC/EC. Furthermore,
217 performing this experiment in a greater number of cell lines would provide improved insight into the spectrum of responses
218 across various EWS cases. Finally, this work could be improved by examining how collateral drug response in EWS changes
219 during relaxed selection after many drug cycles of the treatment regimen have been applied.²⁷ This would represent a model
220 that is even more consistent with refractory EWS in a clinical setting, as patients with refractory disease will often have a gap

221 between the initial standard treatment and the selection of second-line treatments.

222 Despite these caveats, this work provides valuable insight into the evolution of collateral resistance and sensitivity in EWS
223 throughout exposure to standard treatment. Although, many studies have examined the role that collateral sensitivity and
224 resistance play in therapeutic response, they frequently ignore intermediate time points during the development of resistance to
225 a primary treatment. In this work, we aimed to examine collateral sensitivity and resistance across time during development of
226 therapeutic resistance to EWS standard-of-care. We believe this is the first temporal map of collateral sensitivity and resistance
227 in a solid tumor cell line. Using this map, we can see that the path towards collateral sensitivity is not always repeatable, nor is
228 there always a clear trajectory towards resistance or sensitivity. Gene expression signatures can provide clarity when choosing a
229 new treatment in the setting of a tumultuous trajectory towards the evolution of collateral sensitivity or resistance.

230 **Methods**

231 **Materials**

232 EWS cells (A673 and TTC466 cells) were generous gifts from Dr. Stephen Lessnick at Nationwide Children's Hospital,
233 Columbus, OH. 4-hydroperoxycyclophosphamide and sodium thiosulfate were purchased from Toronto Research Chemicals
234 (North York, ON, Canada). Dactinomycin, SP-2509, doxorubicin, etoposide, temozolomide, pazopanib, olaparib, SAHA, and
235 vincristine were products of Cayman Chemical (Ann Arbor, MI). SN-38 was obtained from SelleckChem.com (Houston, TX).
236 The classifications and abbreviations used for all these compounds are found in Table 1.

237 **Cell culture**

238 A673 cells were maintained in Dulbecco's Modified Eagle Medium (D-MEM) supplemented with 10% Fetal Bovine Serum
239 (FBS) and penicillin and streptomycin at 37°C under humidified atmosphere containing 5% CO₂. TTC466 cells were cultured
240 in the same way except Roswell Park Memorial Institute (RPMI) medium was used instead of D-MEM.

241 ***In vitro* combination drug treatments to induce drug resistance**

242 Through drug toxicity assays, we determined EC₅₀ concentrations of chemotherapeutics that are used as standard-of-care to treat
243 EWS.³ This standard-of-care treatment for EWS consists of a vincristine-doxorubicin-cyclophosphamide (VDC) combination
244 cycle followed by an etoposide-ifosfamide (EI) combination cycle. However, both cyclophosphamide and ifosfamide are
245 prodrugs, requiring metabolic activation by an *in vivo* model. In the VDC drug combination, cyclophosphamide is replaced by
246 4-hydroxycyclophosphamide, an activated form of cyclophosphamide; however, there is no such commercially available option
247 for ifosfamide. As ifosfamide is an analog of cyclophosphamide, it was also replaced by 4-hydroperoxycyclophosphamide,
248 due to their similar chemical structures and mechanisms of action. Therefore, we recapitulate Ewing's sarcoma standard-
249 of-care treatment regimen *in vitro* by cycling vincristine-doxorubicin-4-hydroxycyclophosphamide (VDC) and etoposide-4-
250 hydroxycyclophosphamide (EC). The EC₅₀ values were vincristine (0.8 and 0.9 nM), doxorubicin (0.015 and 0.023 nM),
251 4-hydroxycyclophosphamide (0.001 and 0.001 % by volume), and etoposide (0.7 and 0.37 μM) in the A673 and TTC466 cell
252 lines, respectively.

253 In order to induce drug resistance in the A673 and TTC466 cell lines, each cell line was plated as 8 biological (evolutionary)
254 replicates, where 5 experimental replicates were exposed to the drug combination cycles, described below, and 3 control
255 replicates were maintained in dimethyl sulfoxide (DMSO). Due to contamination, one of the experimental replicates (Replicate
256 2) in the A673 cell line was discontinued. Experimental replicates were exposed to the standard-of-care drug cycles, as
257 illustrated in Figure 1. Cells (2 × 10⁶ cells/10cm plate) were first exposed to a combination of vincristine, doxorubicin, and
258 4-hydroxycyclophosphamide at their EC₅₀ concentrations. After 5 days of incubation, the medium was changed to maintenance
259 medium without drugs. After they proliferate to sub-confluent density, a 10 cm plate was set for the next cycle with etoposide
260 and 4-hydroxycyclophosphamide at their initial EC₅₀ concentrations for 5 days, 96-well plates were set for drug sensitivity
261 assay, and a fraction of cells were snap frozen for RNA extraction. Again, as the treated cultures grew to sub-confluence, this
262 cycle was repeated with alternate exposure to the two drug combinations, along with drug sensitivity assays and sampling for
263 RNA extraction between each drug cycle. On the fifth application of the VDC drug combination, the concentration of the drug
264 combination was increased to 6 nM, 0.05 mM, and 0.006% by volume for vincristine, doxorubicin, and cyclophosphamide,
265 respectively.

266 **Drug toxicity assay**

267 Cells were plated into 96-well plates at the density of 6,000 cells/90μl/well. The next day, 10 μl of medium containing various
268 concentrations of drug of interest were added to each well. The final concentration of DMSO used as solvent was kept constant
269 (0.1% by volume for dactinomycin, SP2509, doxorubicin, etoposide, olaparib, SAHA, SN38, and vincristine; and 1% by
270 volume for temozolomide and pazopanib).

271 4-hydroxycyclophosphamide was prepared freshly just prior to each assay by incubating 1 mg of 4-hydroperoxycyclophosphamide
272 with 100 μ L of water containing 1 mg sodium thiosulfate at room temperature for 30 sec, converting 4-hydroperoxycyclophosphamide
273 to 4-hydroxycyclophosphamide. The resulting solution was used for toxicity assay starting with 0.2% (by volume) as
274 the highest concentration. Matching dilution series of sodium thiosulfate solution was assessed as a control to assess 4-
275 hydroxycyclophosphamide toxicity, again using 0.2% (by volume) as the highest concentration.

276 After five days of incubation, cell viability of each well was determined by measuring the enzymatic conversion of
277 alamarBlue (Bio-Rad, Hercules, CA).²⁸ After addition of alamarBlue solution (10 μ l/well), the plate was incubated for two
278 to four hours and the fluorescence intensity (excitation 560 nm / emission 590 nm) of each well was detected by Symphony
279 H2(BioTek, Winooski, VT), a multi-well plate reader. Background fluorescence was determined by measuring the wells without
280 cells incubated with alamarBlue.

281 **Drug response modeling and EC50 estimation**

282 Net alamarBlue conversion for each well was calculated by subtracting the average background fluorescence from each of the
283 fluorescence values. A four-parameter log-logistic (LL.4) model (Hill function) was fit for each biological replicate, performed
284 in triplicate, using the drm function from the drc package in R. This function models the survival measure $S(X)$ at a given dose
285 X as

$$S(X) = b + \frac{b - a}{1 + \left(\frac{EC50}{X}\right)^H}$$

286 where $S(X)$ is the expected response at dose X , a is the minimum response (when dose = 0), b is the highest response (when
287 dose = ∞), $EC50$ is the point of inflection (dose at which 50% of the response occurs), and H (known as the Hill slope) is the
288 steepest part of the curve.²⁹ A negative value for H , as seen in these models, denotes a descending curve, while a positive H
289 represents an ascending curve. Estimated EC50 from these models was solved using the ED function from the drc package
290 (version 3.0.1) in R.

291 **RNA extraction and sequencing**

292 Ribosomal-RNA depleted RNA was prepared from 18 samples of interest using RiboMinus Eukaryote Kit (ThermoFisher,
293 Waltham, MA). RNA sequencing was performed at the Genomic Core, the Lerner Research Institute (Cleveland, OH) with
294 HiSeq 2500 (Illumina, San Diego, CA). Quality control and read trimming was performed using fastp v0.20.0.³⁰ Read alignment
295 was done using STAR v2.7.1 and alignment quantification was done using salmon v0.14.1 against gencode v31 transcript
296 set with average 12 million reads per sample.³¹⁻³³ Transcript level abundance estimates were then converted to gene level
297 estimated counts using tximport R package.³⁴

298 **Differential gene expression analysis**

299 Samples sent for sequencing were ranked based on their EC50 to each drug. For each drug analyzed, differential gene expression
300 (DE) analysis compared samples in the top and bottom third of the ranked EC50 values. This DE analysis was performed using
301 the EBSeq R package (version 1.24.0), with a false discovery threshold of 0.05 and the maxround parameter set to 15.^{35,36}

302 Acknowledgements

303 JGS would like to thank the NIH Loan Repayment Program for their generous support, the Paul Calabresi Career Development
304 Award for Clinical Oncology (NIH K12CA076917), the Carson Sarcoma Foundation, and Chemowarrior Foundation. Addi-
305 tionally, JAS thanks the NIH for support through the T32GM007250 grant. The authors thank the Lerner Research Institute
306 Genomic Core for RNA-sequencing, and the Stephen Lessnick and Kathleen Pishas for helpful discussions and for sharing the
307 cell lines.
308

309 Author contributions statement

310 JAS performed data processing, wrote all associated code,
311 analyzed the data, and wrote the manuscript. EM and MH
312 performed the long term evolution experiments, drug sensi-
313 tivity assays, RNA extraction, and wrote the manuscript. A.
314 Dhawan contributed to experimental design and analyzed
315 the data. A. Durmaz performed RNA-sequencing quality
316 control and alignment. PA contributed to experimental de-
317 sign and analyzed the data. JGS analyzed the data and
318 wrote the manuscript. These contributions are graphically
319 illustrated in Figure 5.

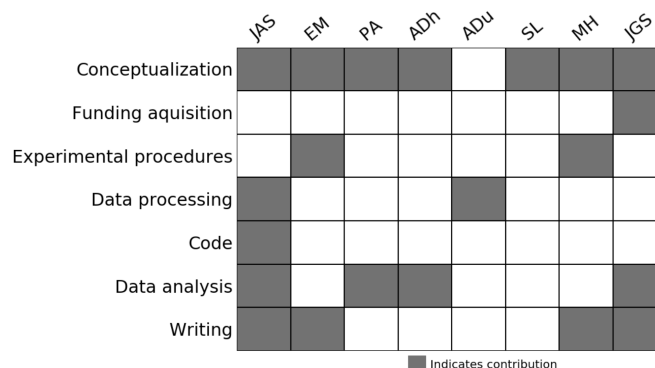


Figure 5. Author Contributions

320 Declaration of Interests

321 Stephen Lessnick serves as a Scientific Advisor for Salarius
322 Pharmaceuticals.

323 Code availability

324 The code to perform the statistical analysis is available via GitHub at
325 <https://github.com/jessicascarborough/ES-CS-evolution>.

References

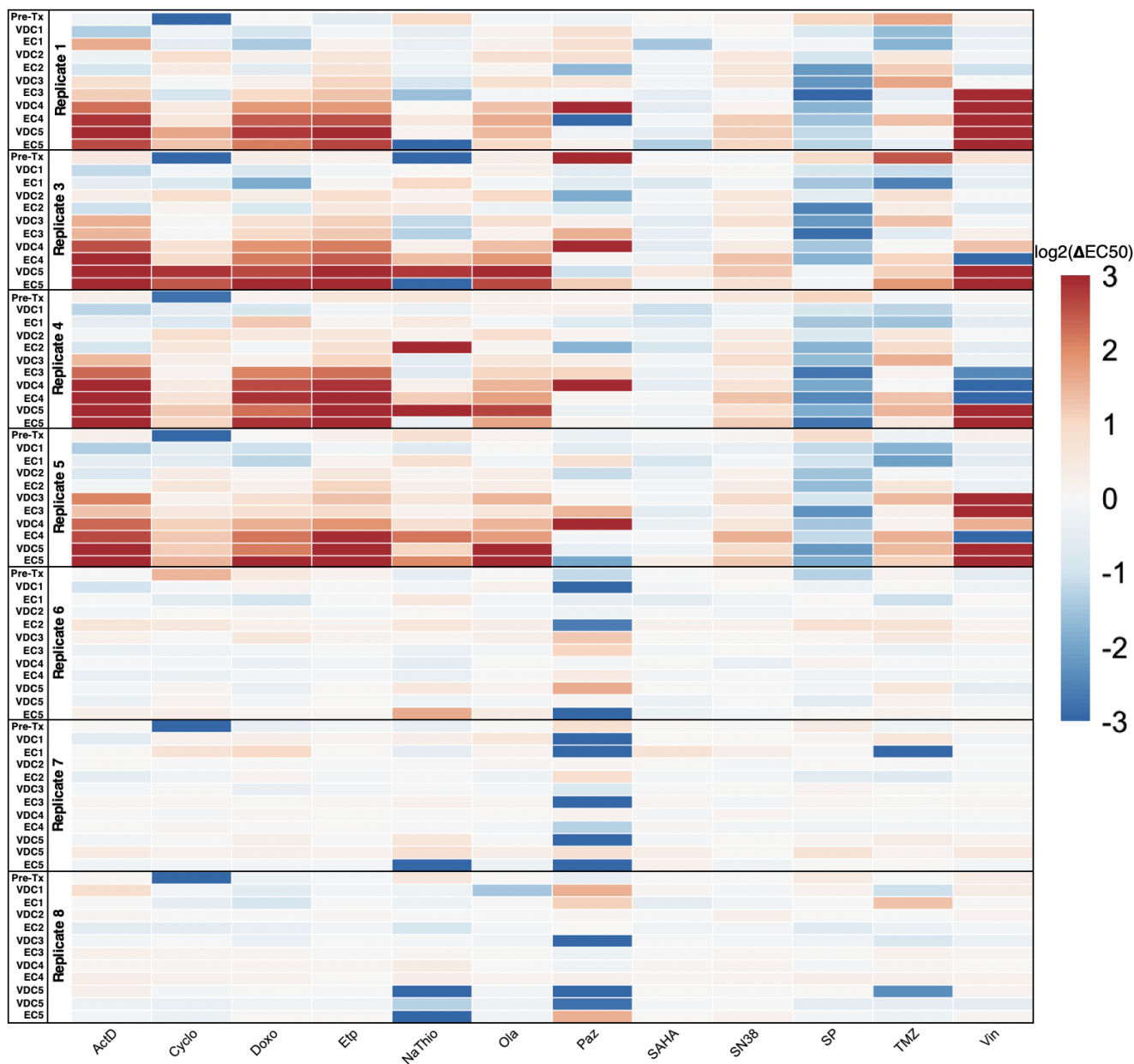
- 327 1. Ries, L. A. G. *Cancer incidence and survival among children and adolescents: United States SEER program, 1975-1995*.
328 99 (National Cancer Institute, 1999).
- 329 2. Esiashvili, N., Goodman, M. & Marcus, R. B. Changes in incidence and survival of ewing sarcoma patients over the past 3
330 decades: Surveillance epidemiology and end results data. *J. pediatric hematology/oncology* **30**, 425–430 (2008).
- 331 3. Grier, H. E. *et al.* Addition of ifosfamide and etoposide to standard chemotherapy for ewing’s sarcoma and primitive
332 neuroectodermal tumor of bone. *New Engl. J. Medicine* **348**, 694–701 (2003).
- 333 4. Hunold, A. *et al.* Topotecan and cyclophosphamide in patients with refractory or relapsed ewing tumors. *Pediatr. blood &*
334 *cancer* **47**, 795–800 (2006).
- 335 5. Huang, M. & Lucas, K. Current therapeutic approaches in metastatic and recurrent ewing sarcoma. *Sarcoma* **2011** (2010).
- 336 6. Womer, R. B. *et al.* Randomized controlled trial of interval-compressed chemotherapy for the treatment of localized ewing
337 sarcoma: a report from the children’s oncology group. *J. Clin. Oncol.* **30**, 4148 (2012).
- 338 7. Ahmed, A. A., Zia, H. & Wagner, L. Therapy resistance mechanisms in ewing’s sarcoma family tumors. *Cancer*
339 *chemotherapy pharmacology* **73**, 657–663 (2014).
- 340 8. Pluchino, K. M., Hall, M. D., Goldsborough, A. S., Callaghan, R. & Gottesman, M. M. Collateral sensitivity as a strategy
341 against cancer multidrug resistance. *Drug Resist. Updat.* **15**, 98–105 (2012).
- 342 9. Pál, C., Papp, B. & Lázár, V. Collateral sensitivity of antibiotic-resistant microbes. *Trends microbiology* **23**, 401–407
343 (2015).
- 344 10. Hall, M. D., Handley, M. D. & Gottesman, M. M. Is resistance useless? multidrug resistance and collateral sensitivity.
345 *Trends pharmacological sciences* **30**, 546–556 (2009).
- 346 11. Nichol, D. *et al.* Antibiotic collateral sensitivity is contingent on the repeatability of evolution. *Nat. communications* **10**,
347 1–10 (2019).
- 348 12. Imamovic, L. & Sommer, M. O. Use of collateral sensitivity networks to design drug cycling protocols that avoid resistance
349 development. *Sci. translational medicine* **5**, 204ra132–204ra132 (2013).
- 350 13. Munck, C., Gumpert, H. K., Wallin, A. I. N., Wang, H. H. & Sommer, M. O. Prediction of resistance development against
351 drug combinations by collateral responses to component drugs. *Sci. translational medicine* **6**, 262ra156–262ra156 (2014).
- 352 14. Zhao, B. *et al.* Exploiting temporal collateral sensitivity in tumor clonal evolution. *Cell* **165**, 234–246 (2016).
- 353 15. Dhawan, A. *et al.* Collateral sensitivity networks reveal evolutionary instability and novel treatment strategies in alk
354 mutated non-small cell lung cancer. *Sci. Reports* **7**, 1–9 (2017).
- 355 16. Maltas, J. & Wood, K. B. Pervasive and diverse collateral sensitivity profiles inform optimal strategies to limit antibiotic
356 resistance. *PLoS biology* **17** (2019).
- 357 17. Szuhai, K., IJszenga, M., Tanke, H. J., Rosenberg, C. & Hogendoorn, P. C. Molecular cytogenetic characterization of four
358 previously established and two newly established ewing sarcoma cell lines. *Cancer genetics cytogenetics* **166**, 173–179
359 (2006).
- 360 18. Martinez-Ramirez, A. *et al.* Characterization of the a673 cell line (ewing tumor) by molecular cytogenetic techniques.
361 *Cancer genetics cytogenetics* **141**, 138–142 (2003).
- 362 19. Sankar, S. *et al.* Reversible lsd1 inhibition interferes with global ews/ets transcriptional activity and impedes ewing sarcoma
363 tumor growth. *Clin. cancer research* **20**, 4584–4597 (2014).
- 364 20. Fleming, R. A. An overview of cyclophosphamide and ifosfamide pharmacology. *Pharmacother. The J. Hum. Pharmacol.*
365 *Drug Ther.* **17**, 146S–154S (1997).
- 366 21. Chen, K. G. & Sikic, B. I. Molecular pathways: regulation and therapeutic implications of multidrug resistance. *Clin.*
367 *cancer research* **18**, 1863–1869 (2012).
- 368 22. Gatti, L. *et al.* Histone deacetylase inhibitor-temozolomide co-treatment inhibits melanoma growth through suppression of
369 chemokine (cc motif) ligand 2-driven signals. *Oncotarget* **5**, 4516 (2014).
- 370 23. O’Leary, N. A. *et al.* Reference sequence (refseq) database at ncbi: current status, taxonomic expansion, and functional
371 annotation. *Nucleic acids research* **44**, D733–D745 (2016).
- 372 24. Yang, G.-J., Lei, P.-M., Wong, S.-Y., Ma, D.-L. & Leung, C.-H. Pharmacological inhibition of lsd1 for cancer treatment.
373 *Molecules* **23**, 3194 (2018).

- 374 **25.** Klug, A. Zinc finger peptides for the regulation of gene expression. *J. molecular biology* **293**, 215–218 (1999).
- 375 **26.** Hampsey, M. & Reinberg, D. Transcription: why are tafs essential? *Curr. Biol.* **7**, R44–R46 (1997).
- 376 **27.** Card, K. J., LaBar, T., Gomez, J. B. & Lenski, R. E. Historical contingency in the evolution of antibiotic resistance after
377 decades of relaxed selection. *PLoS biology* **17** (2019).
- 378 **28.** Hamid, R., Rotshteyn, Y., Rabadi, L., Parikh, R. & Bullock, P. Comparison of alamar blue and mtt assays for high
379 through-put screening. *Toxicol. vitro* **18**, 703–710 (2004).
- 380 **29.** Gadagkar, S. R. & Call, G. B. Computational tools for fitting the hill equation to dose–response curves. *J. Pharmacol.*
381 *Toxicol. methods* **71**, 68–76 (2015).
- 382 **30.** Chen, S., Zhou, Y., Chen, Y. & Gu, J. fastp: an ultra-fast all-in-one fastq preprocessor. *Bioinformatics* **34**, i884–i890
383 (2018).
- 384 **31.** Dobin, A. *et al.* Star: ultrafast universal rna-seq aligner. *Bioinformatics* **29**, 15–21 (2013).
- 385 **32.** Patro, R., Duggal, G., Love, M. I., Irizarry, R. A. & Kingsford, C. Salmon provides fast and bias-aware quantification of
386 transcript expression. *Nat. methods* **14**, 417 (2017).
- 387 **33.** Harrow, J. *et al.* Gencode: the reference human genome annotation for the encode project. *Genome research* **22**, 1760–1774
388 (2012).
- 389 **34.** Sonesson, C., Love, M. I. & Robinson, M. D. Differential analyses for rna-seq: transcript-level estimates improve gene-level
390 inferences. *F1000Research* **4** (2015).
- 391 **35.** Leng, N. & Kendziorski, C. *EBSeq: An R package for gene and isoform differential expression analysis of RNA-seq data*
392 (2019). R package version 1.24.0.
- 393 **36.** Žibera, A. *Generalized and Classical Blockmodeling of Valued Networks* (2018). R package version 0.3.4.

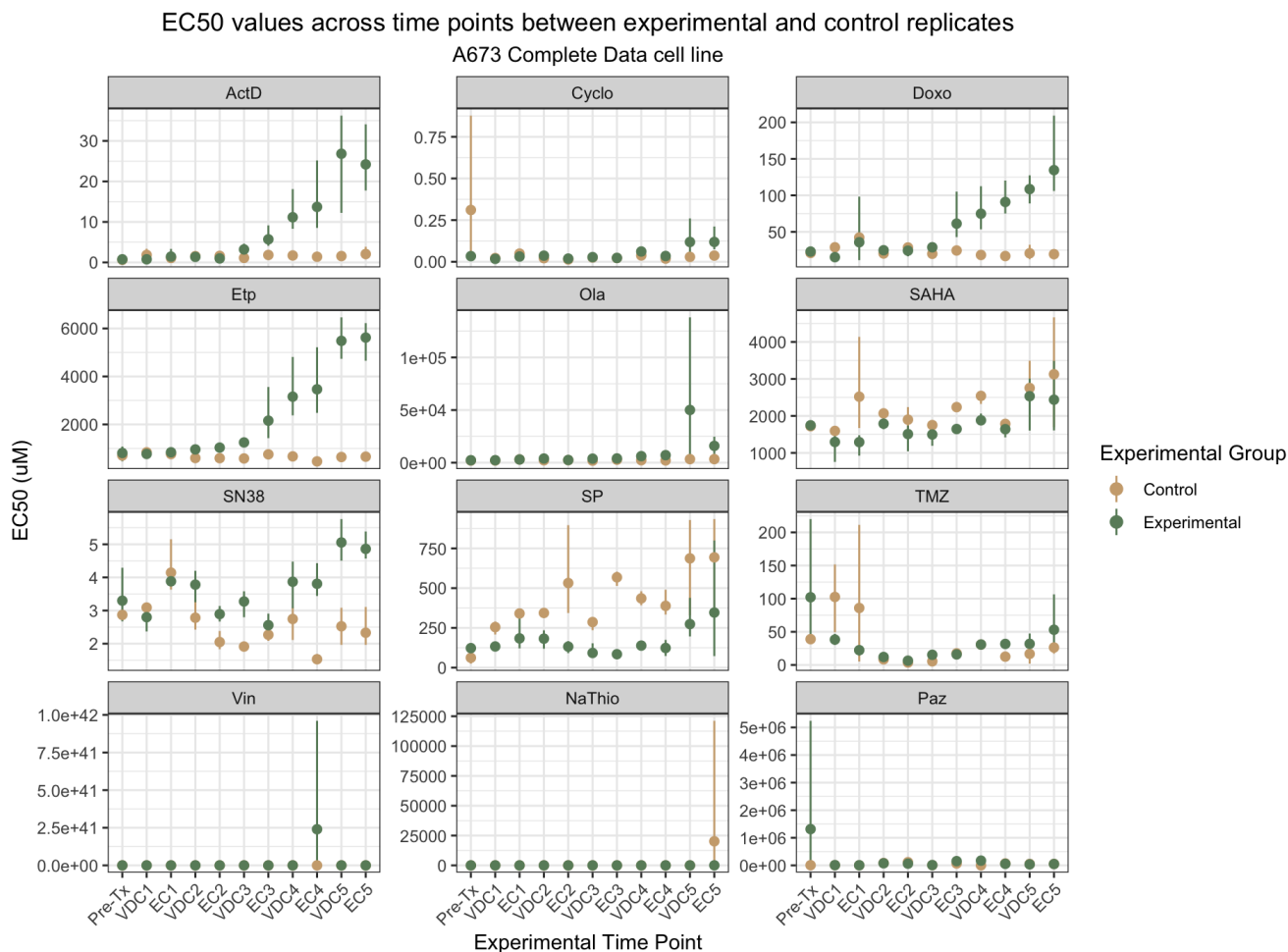
394 Supplementary Information

395 Complete A673 EC50 Data

396 The following plots mirror Figures 2 and 3, respectively. The data does not censor the EC50 for Replicate 5 against olaparib
 397 at the VDC5 timepoint, as seen in Figures 2 and 3. Additionally, the drugs removed from main text analysis, vincristine,
 398 pazopanib, and sodium thiosulfate are included. These drugs were censored in the main text due to poorly fit dose-response
 399 models. Interpretation of these plots can be found in the main text.



Supplementary Figure 1. Uncensored temporal collateral sensitivity map representing EC50 changes to panel of drugs in A673 cell line as it develops resistance to standard treatment A heatmap representing how the EC50 to a panel of nine drugs changes in 4 experimental and 3 control evolutionary replicates from the A673 cell line as they are exposed to the VDC/EC drug combinations over time. Color represents the log₂ fold change of EC50 to a drug (columns) for a replicate at a given evolutionary time point (rows) compared to the average EC50 of the three control evolutionary replicates at the corresponding time point. Time points are denoted as the drug combination that a given replicate has recently recovered from. For example, the data representing dose-response models after the first application of the VDC drug combination would be labeled with VDC1.

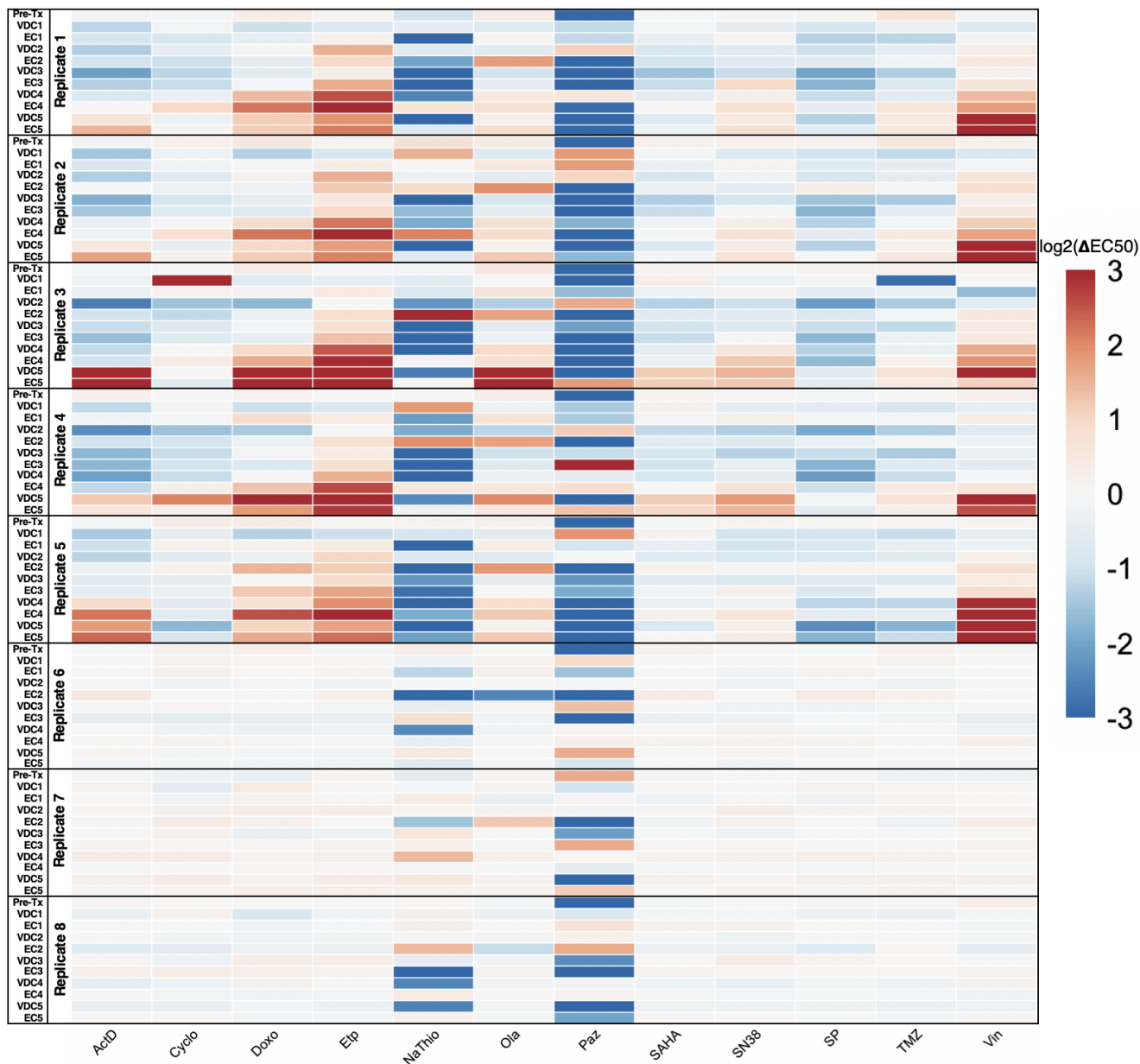


Supplementary Figure 2. Uncensored point-range plots demonstrating EC50 changes in A673 experimental and control replicates over time. Point-range plots representing the changes in drug response to a panel of 12 drugs. Experimental time points (x-axis) represent which step in the drug cycle the replicates have just recovered from. Points on the plot represent the average EC50 for the group, either experimental or control. Lines represent the range for the entire group. The y-axis of all the point-range plots has μM units, except Cyclo and NaThio, where the units are percent by volume.

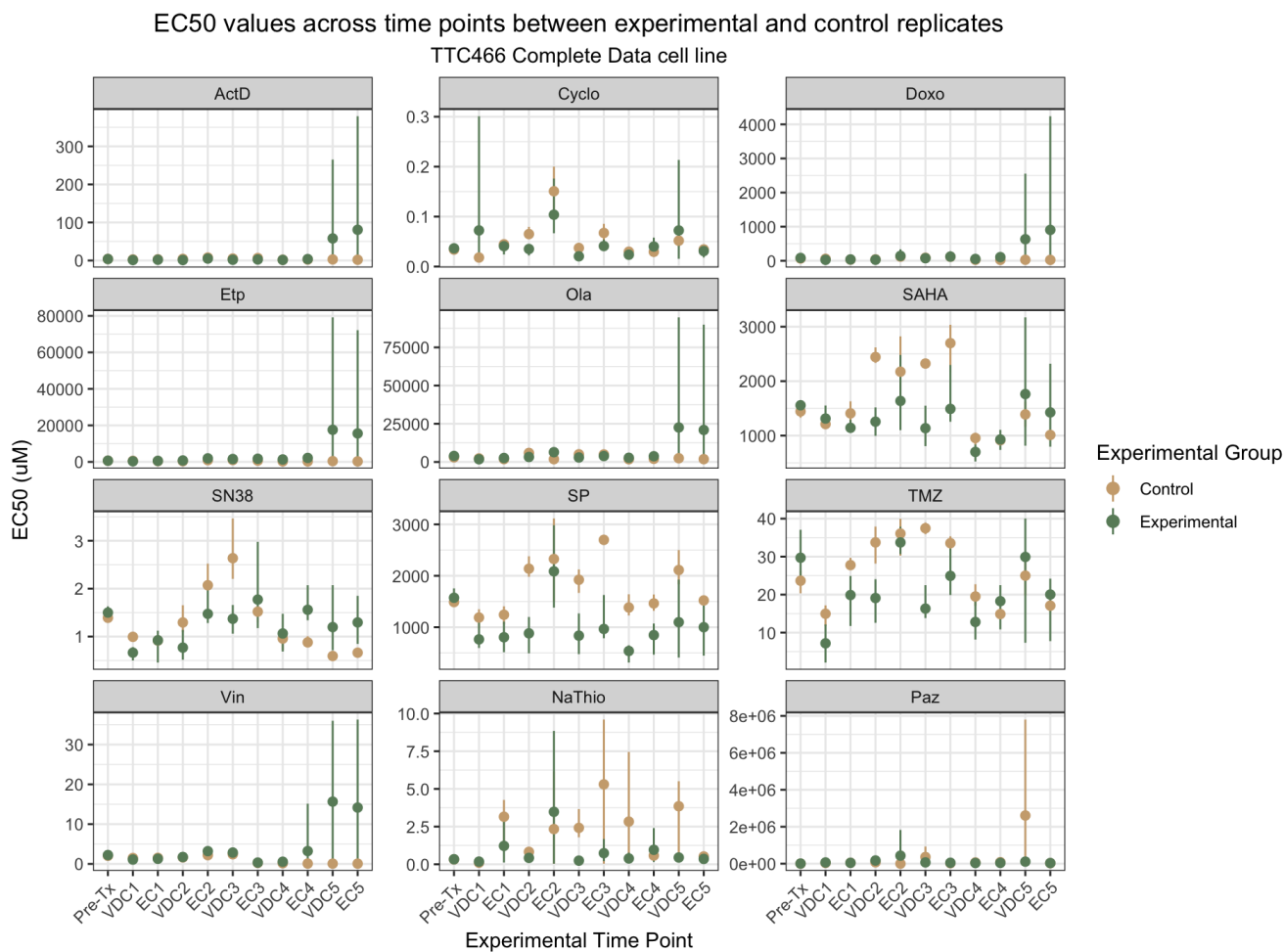
400 **Complete TTC466 EC50 Data**

401 Supplementary Figures 3 and 4 displays the changes in drug response to all 12 agents over time in the TTC466 cell line. In
402 comparing the two cell lines, it is clear that the A673 cell line displays more stable behavior, while TTC466 shows much more
403 variability over time. In other words, as the treatment cycles progress, the A673 cell line tends to move steadily towards a
404 resistant or sensitive state, while the TTC466 cell line tends to fluctuate more. The TTC466 control replicates also tend to have
405 more fluctuation between time points, despite being exposed to only media and having relative agreement between technical
406 replicates. For this reason, we chose to focus our analysis on the A673 cell line, while the TTC466 cell line results can be
407 found in the Supplementary Information.

408 In Supplementary Figure 3, we see that after the first exposure to the VDC drug combination (VDC1) in the TTC466
409 cell line, resistance to cyclophosphamide suddenly emerges. This doesn't occur in any other replicate, nor at any other time
410 point. These findings were confirmed by examining the drug-response curve at this time point to ensure a well-fit model. Two
411 hypotheses for why the replicate didn't retain the cyclophosphamide-resistant trait in the next generation include an equally
412 rapid loss of this trait in the next generations or a bottleneck selection during the procedure where the cells that were resistant
413 to cyclophosphamide were not plated for the next round of the drug treatment cycle. Next, another example of drug-response
414 fluctuation in the TTC466 cell line may have been mistaken as a rare shift in drug response if only one evolutionary replicate
415 had been performed. In Supplementary Figure 3, we see that after the second exposure to the EC combination (EC2), the EC50
416 of every experimental replicate has increased chemoresistance to olaparib before returning to a more sensitive state after the
417 next drug cycle. Supplementary Figure 4, demonstrates that there is a large range in the control replicates at the corresponding
418 time point, which makes the comparison between the experimental and control replicates less reliable; however, it is clear that
419 from the time points before and after EC2, the EC50 increases significantly at EC2.



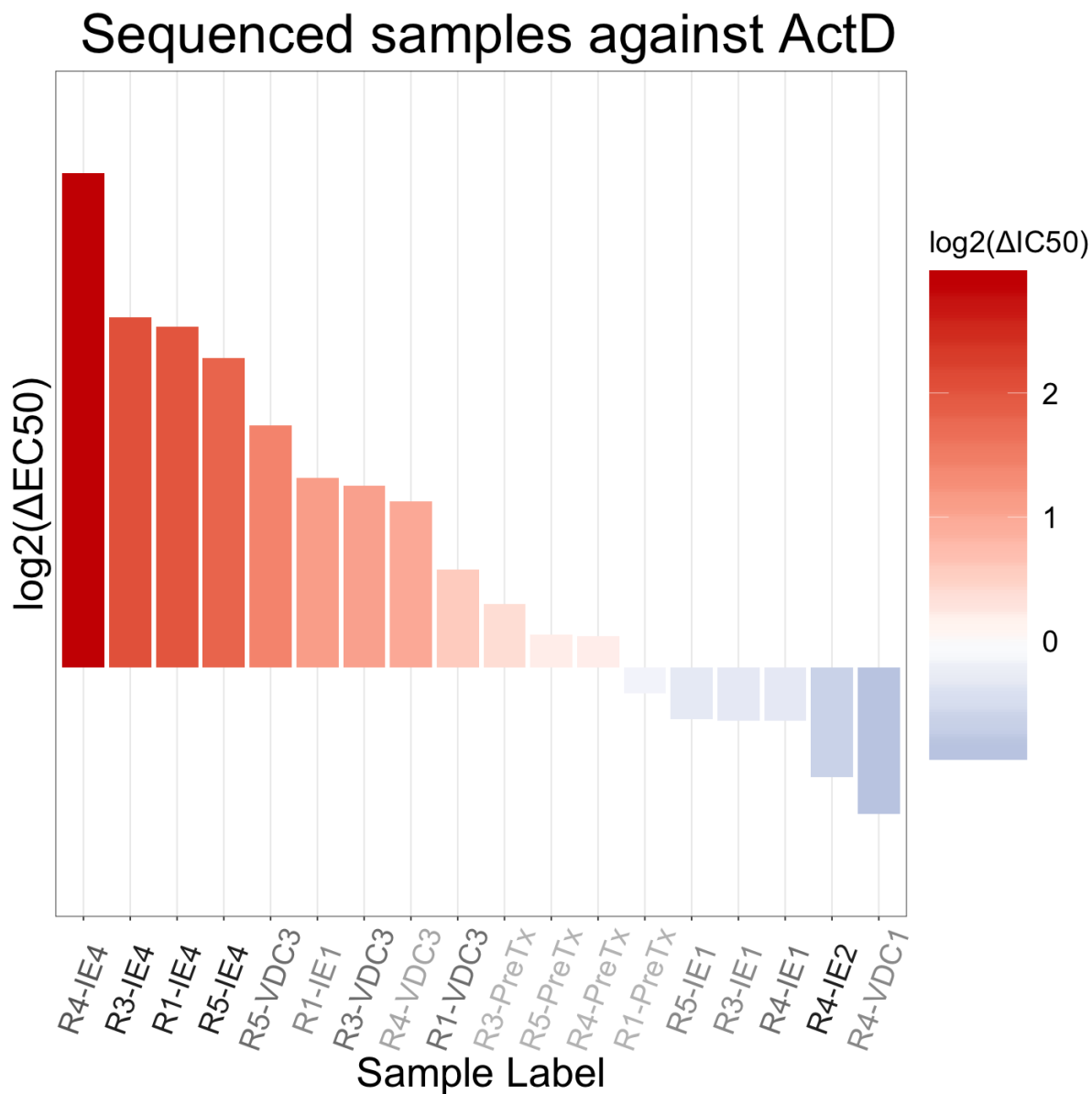
Supplementary Figure 3. Uncensored temporal collateral sensitivity map representing EC₅₀ changes to panel of drugs in TTC466 cell line as it develops resistance to standard treatment A heatmap representing how the EC₅₀ to a panel of nine drugs changes in 5 experimental and 3 control evolutionary replicates from the TTC466 cell line as they are exposed to the VDC/EC drug combinations over time. Color represents the log₂ fold change of EC₅₀ to a drug (columns) for a replicate at a given evolutionary time point (rows) compared to the average EC₅₀ of the three control evolutionary replicates at the corresponding time point. Time points are denoted as the drug combination that a given replicate has recently recovered from. For example, the data representing dose-response models after the first application of the VDC drug combination would be labeled with VDC1.



Supplementary Figure 4. Uncensored point-range plots demonstrating EC50 changes in TTC466 experimental and control replicates over time. Point-range plots representing the changes in drug response to a panel of 12 drugs.

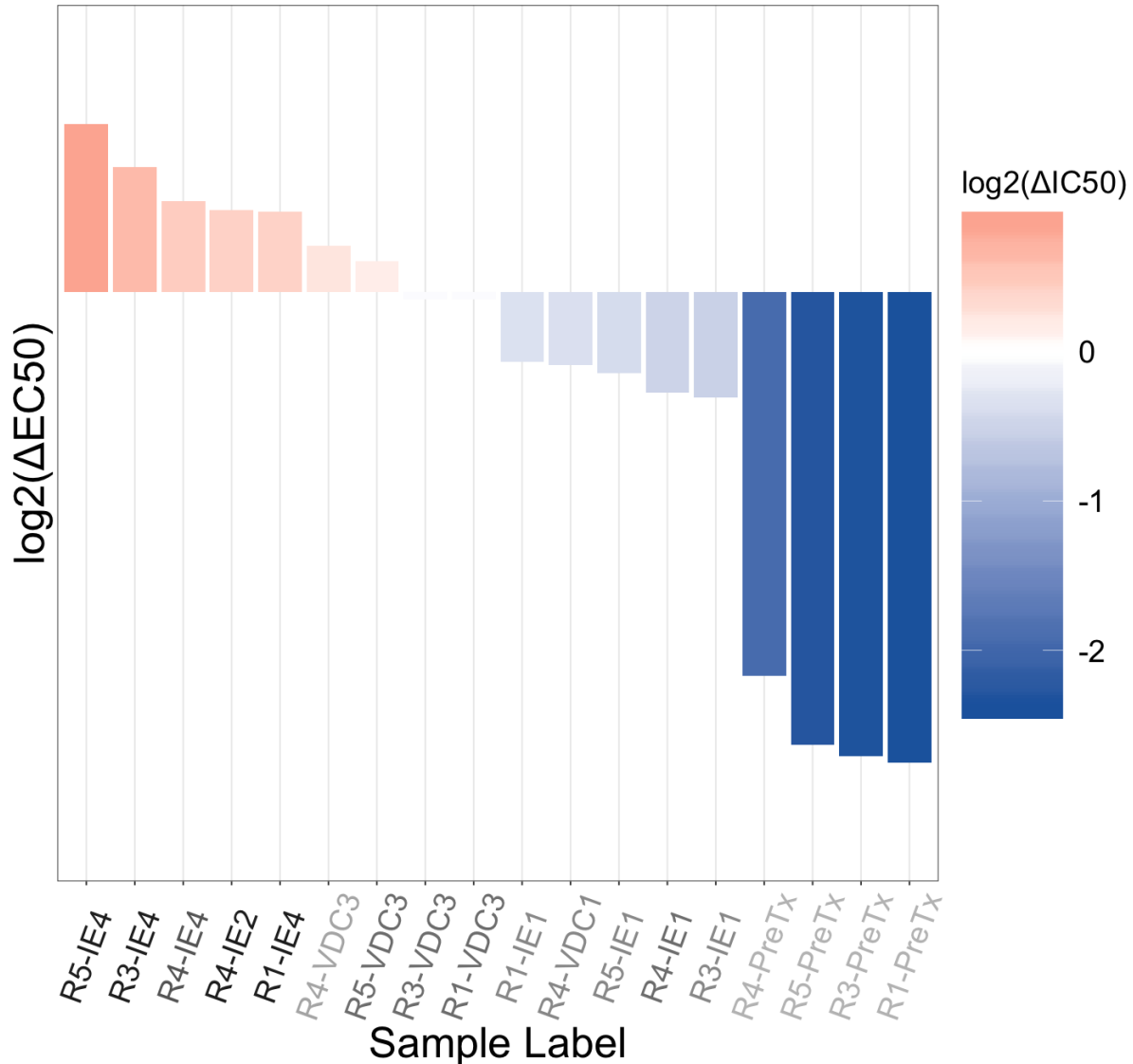
Experimental time points (x-axis) represent which step in the drug cycle the replicates have just recovered from. Points on the plot represent the average EC50 for the group, either experimental or control. Lines represent the range for the entire group. The y-axis of all the point-range plots has uM units, except Cyclo and NaThio, where the units are percent by volume.

420 Waterfall plots for sequenced samples against all drugs

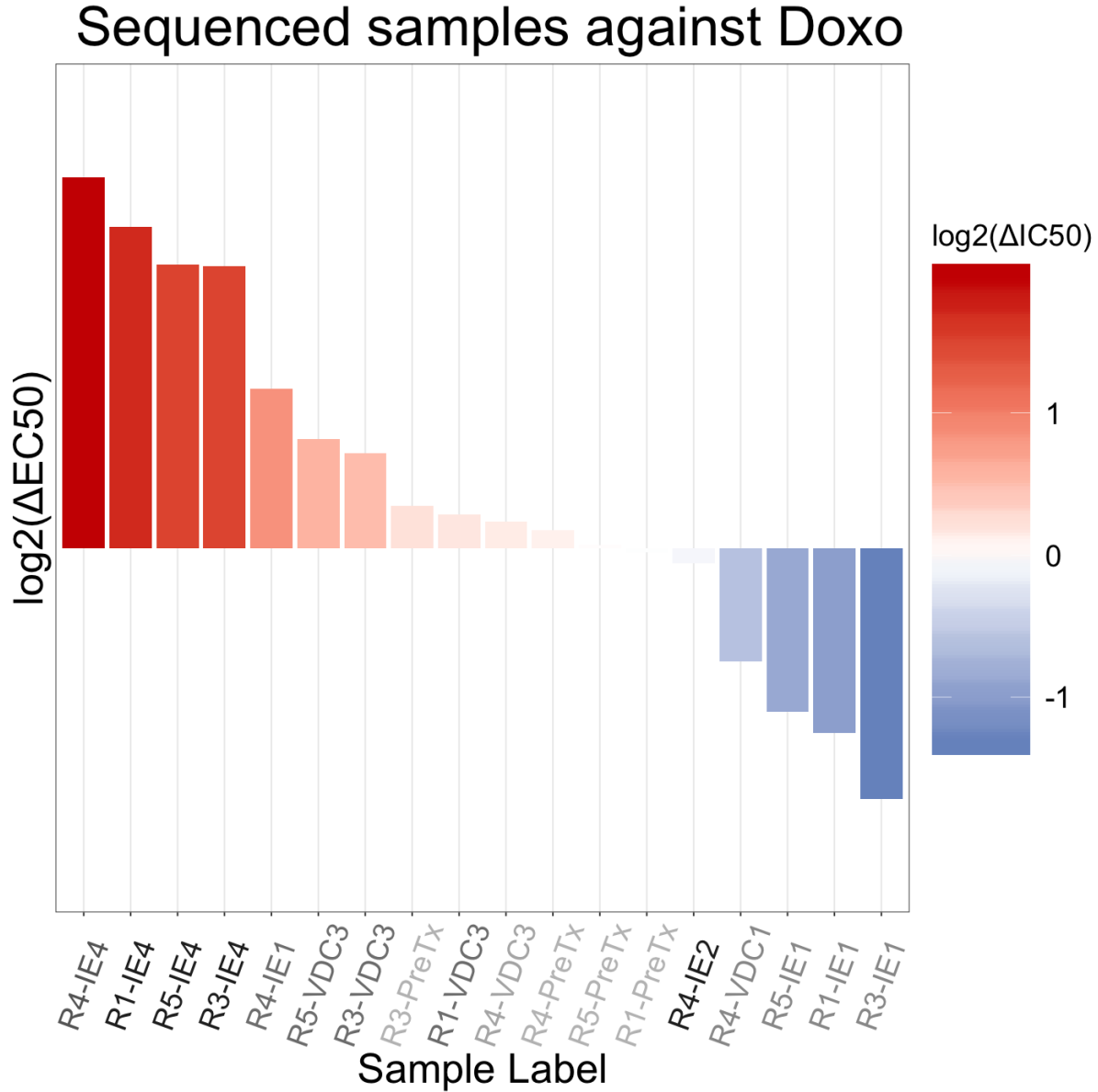


Supplementary Figure 5. Waterfall of EC₅₀ values for sequenced samples against dactinomycin. Color represents \log_2 change in EC₅₀ between the sample and average control EC₅₀ at the given time point. Red shows a change towards resistance, while blue shows a change towards sensitivity. Samples are ranked along the x-axis from least-to-most sensitive. Sample labels on the x-axis are represented by darker colors the longer they have been evolved in the evolutionary experiment.

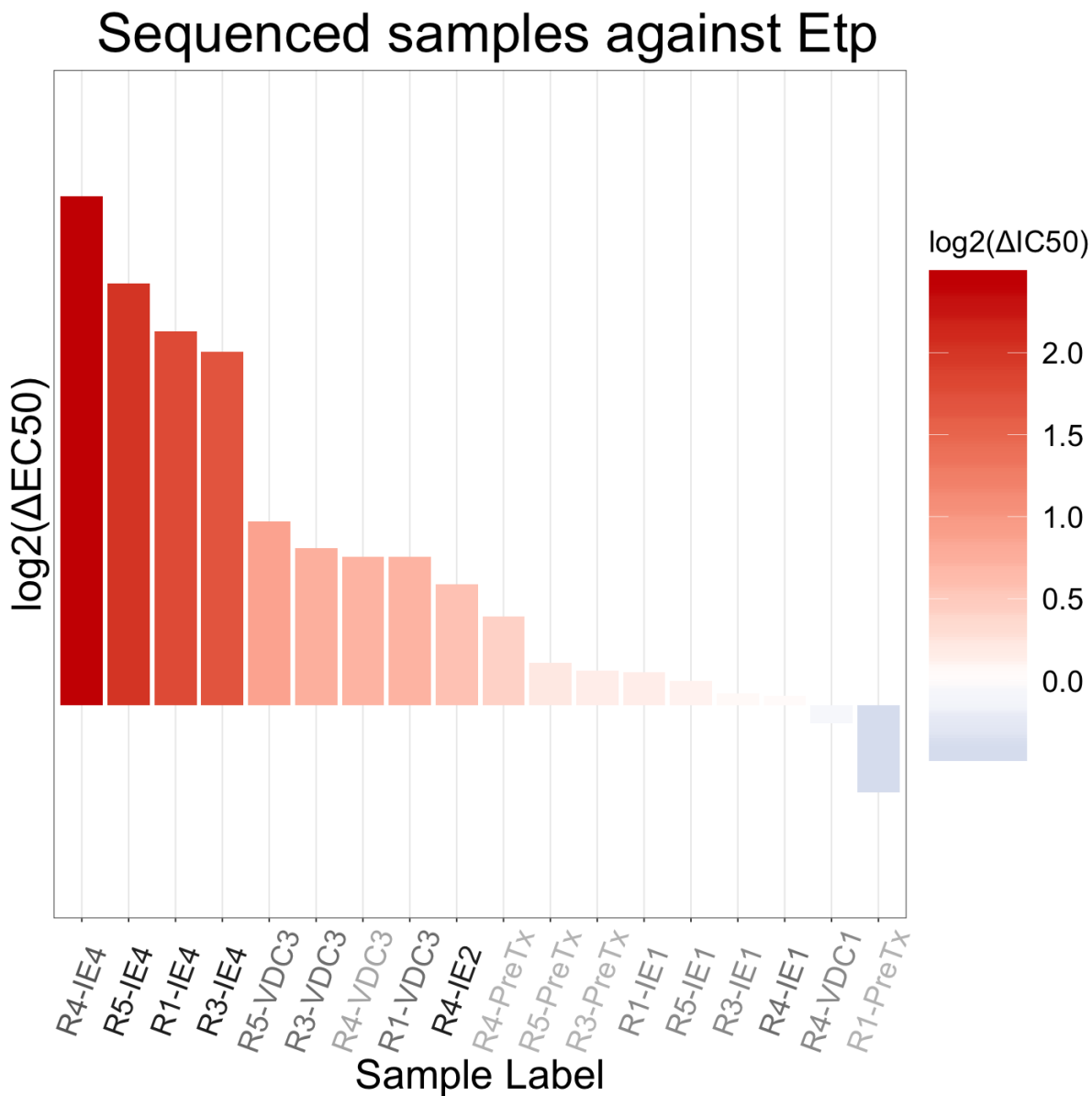
Sequenced samples against Cyclo



Supplementary Figure 6. Waterfall of EC₅₀ values for sequenced samples against cyclophosphamide. Color represents log₂ change in EC₅₀ between the sample and average control EC₅₀ at the given time point. Red shows a change towards resistance, while blue shows a change towards sensitivity. Samples are ranked along the x-axis from least-to-most sensitive. Sample labels on the x-axis are represented by darker colors the longer they have been evolved in the evolutionary experiment.

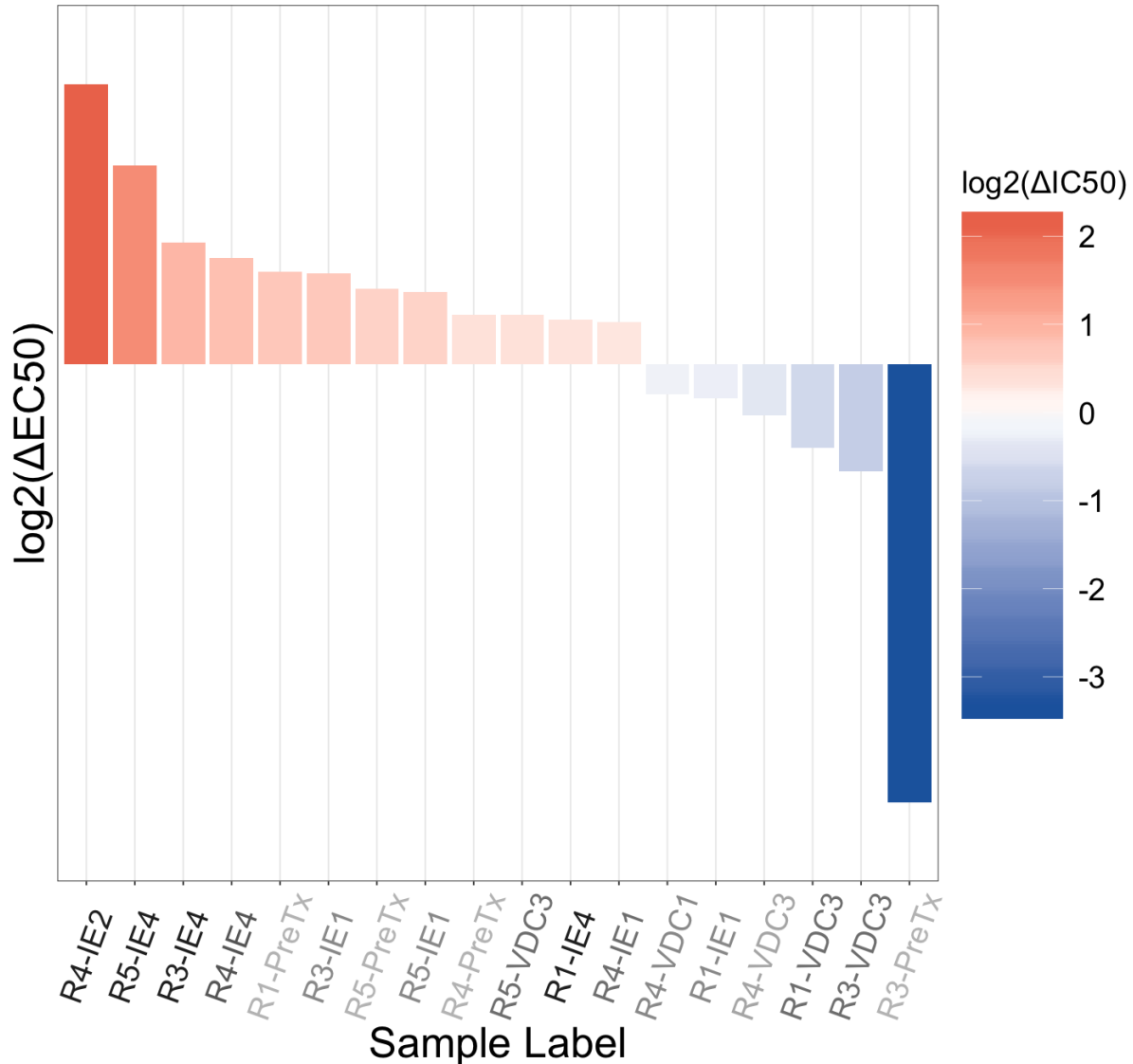


Supplementary Figure 7. Waterfall of EC₅₀ values for sequenced samples against doxorubicin. Color represents \log_2 change in EC₅₀ between the sample and average control EC₅₀ at the given time point. Red shows a change towards resistance, while blue shows a change towards sensitivity. Samples are ranked along the x-axis from least-to-most sensitive. Sample labels on the x-axis are represented by darker colors the longer they have been evolved in the evolutionary experiment.

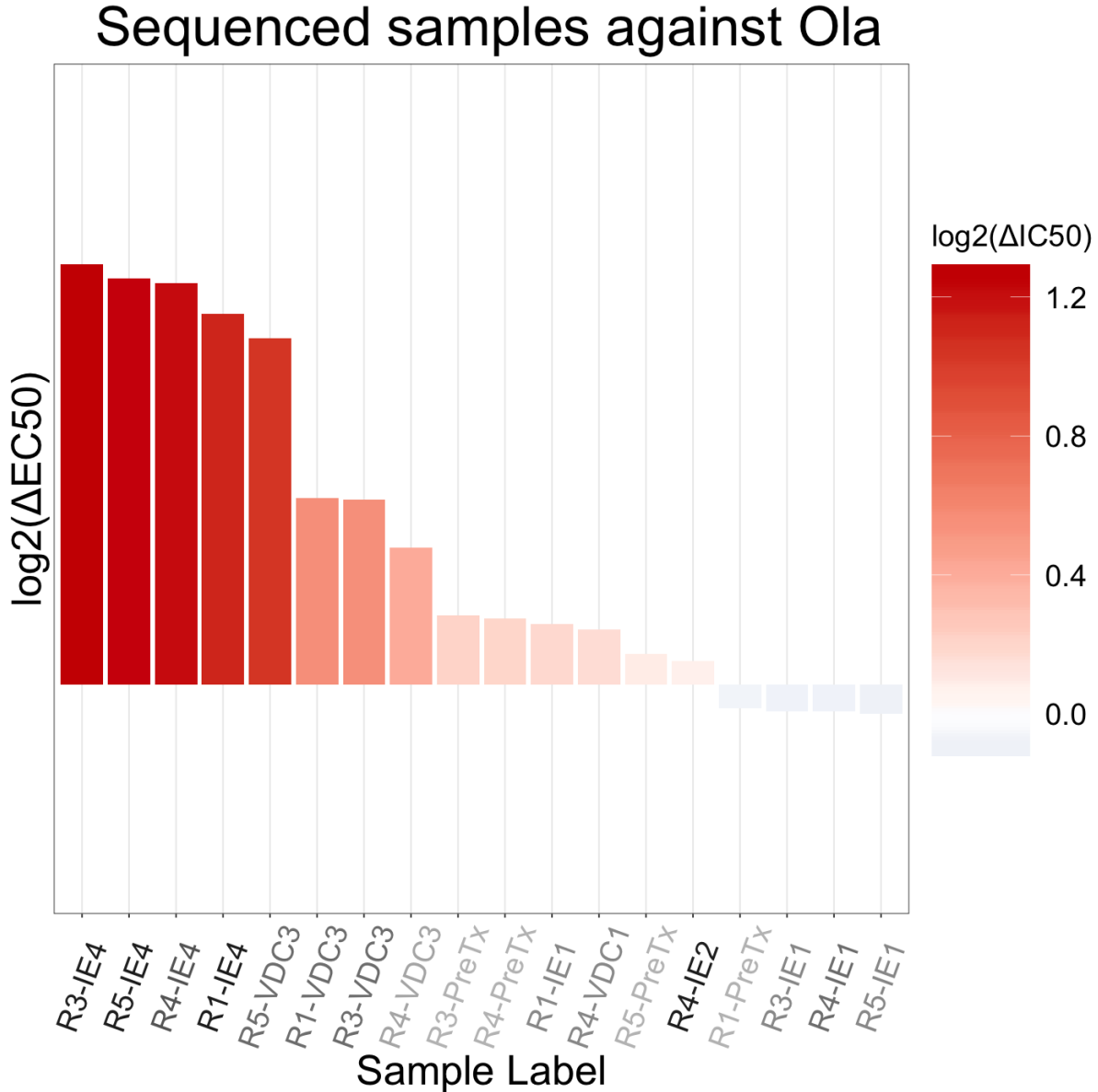


Supplementary Figure 8. Waterfall of EC₅₀ values for sequenced samples against etoposide. Color represents \log_2 change in EC₅₀ between the sample and average control EC₅₀ at the given time point. Red shows a change towards resistance, while blue shows a change towards sensitivity. Samples are ranked along the x-axis from least-to-most sensitive. Sample labels on the x-axis are represented by darker colors the longer they have been evolved in the evolutionary experiment.

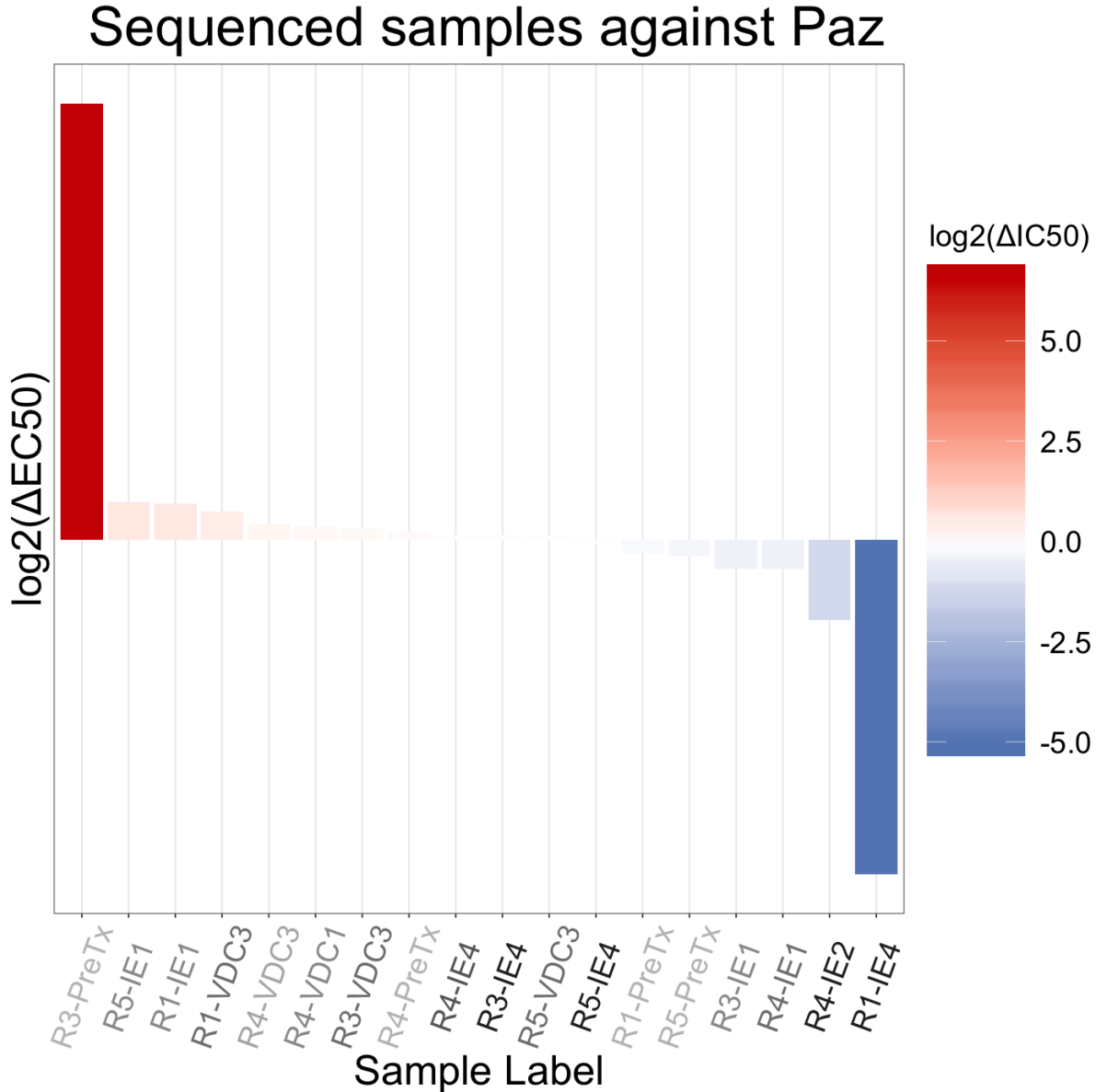
Sequenced samples against NaThio



Supplementary Figure 9. Waterfall of EC₅₀ values for sequenced samples against sodium thiosulfate. Color represents log₂ change in EC₅₀ between the sample and average control EC₅₀ at the given time point. Red shows a change towards resistance, while blue shows a change towards sensitivity. Samples are ranked along the x-axis from least-to-most sensitive. Sample labels on the x-axis are represented by darker colors the longer they have been evolved in the evolutionary experiment.

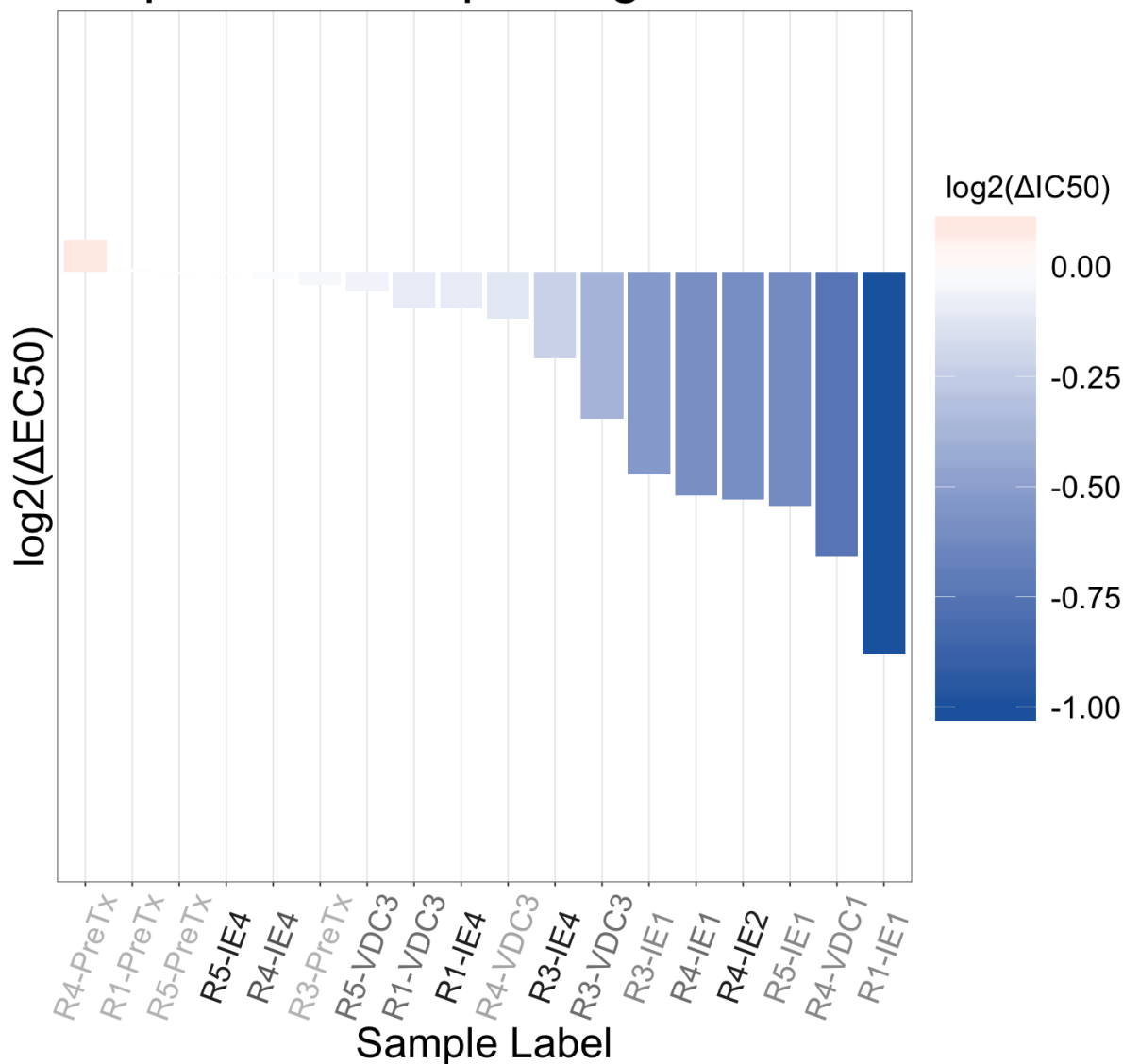


Supplementary Figure 10. Waterfall of EC₅₀ values for sequenced samples against olaparib. Color represents \log_2 change in EC₅₀ between the sample and average control EC₅₀ at the given time point. Red shows a change towards resistance, while blue shows a change towards sensitivity. Samples are ranked along the x-axis from least-to-most sensitive. Sample labels on the x-axis are represented by darker colors the longer they have been evolved in the evolutionary experiment.

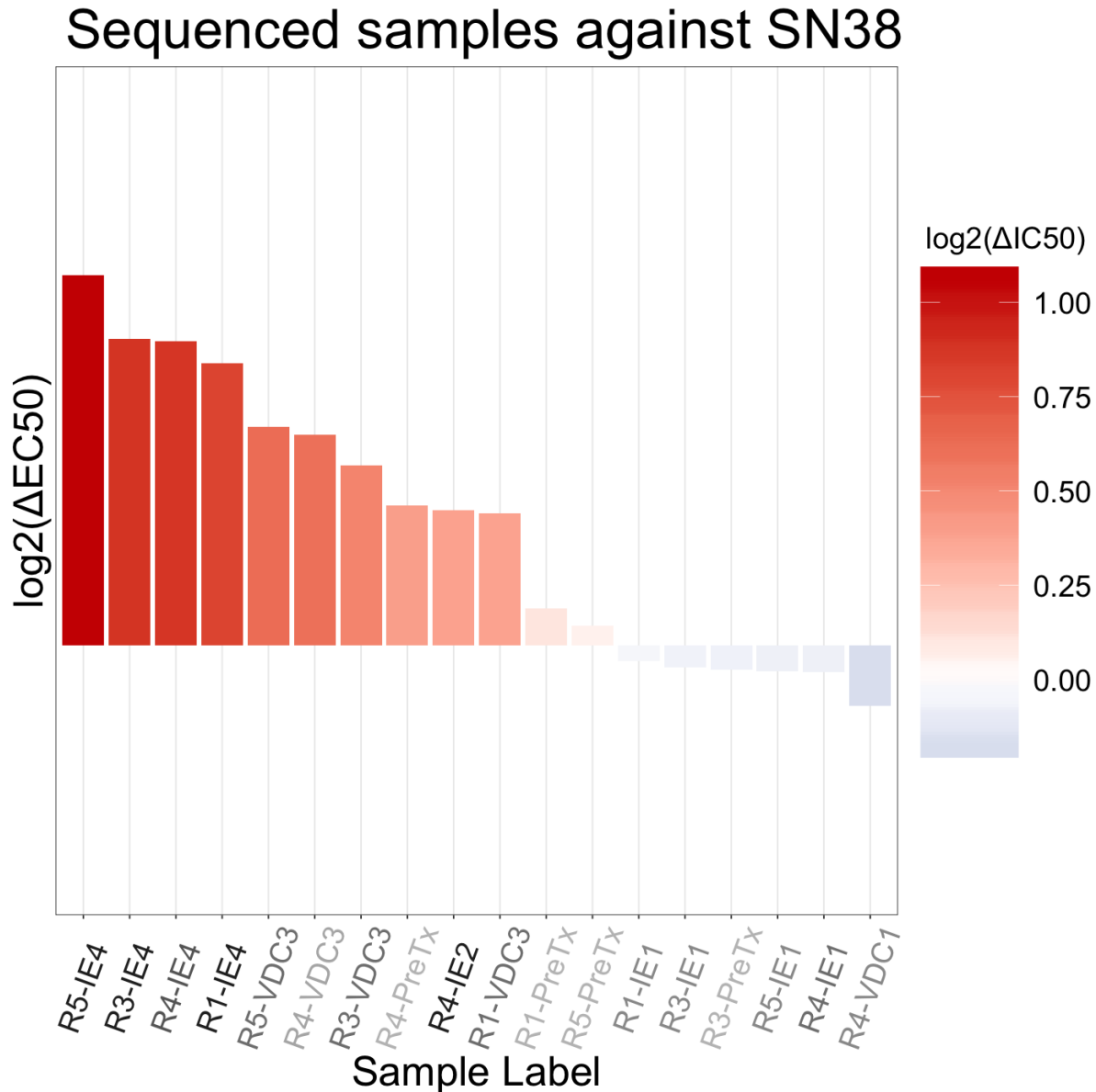


Supplementary Figure 11. Waterfall of EC₅₀ values for sequenced samples against pazopanib. Color represents \log_2 change in EC₅₀ between the sample and average control EC₅₀ at the given time point. Red shows a change towards resistance, while blue shows a change towards sensitivity. Samples are ranked along the x-axis from least-to-most sensitive. Sample labels on the x-axis are represented by darker colors the longer they have been evolved in the evolutionary experiment.

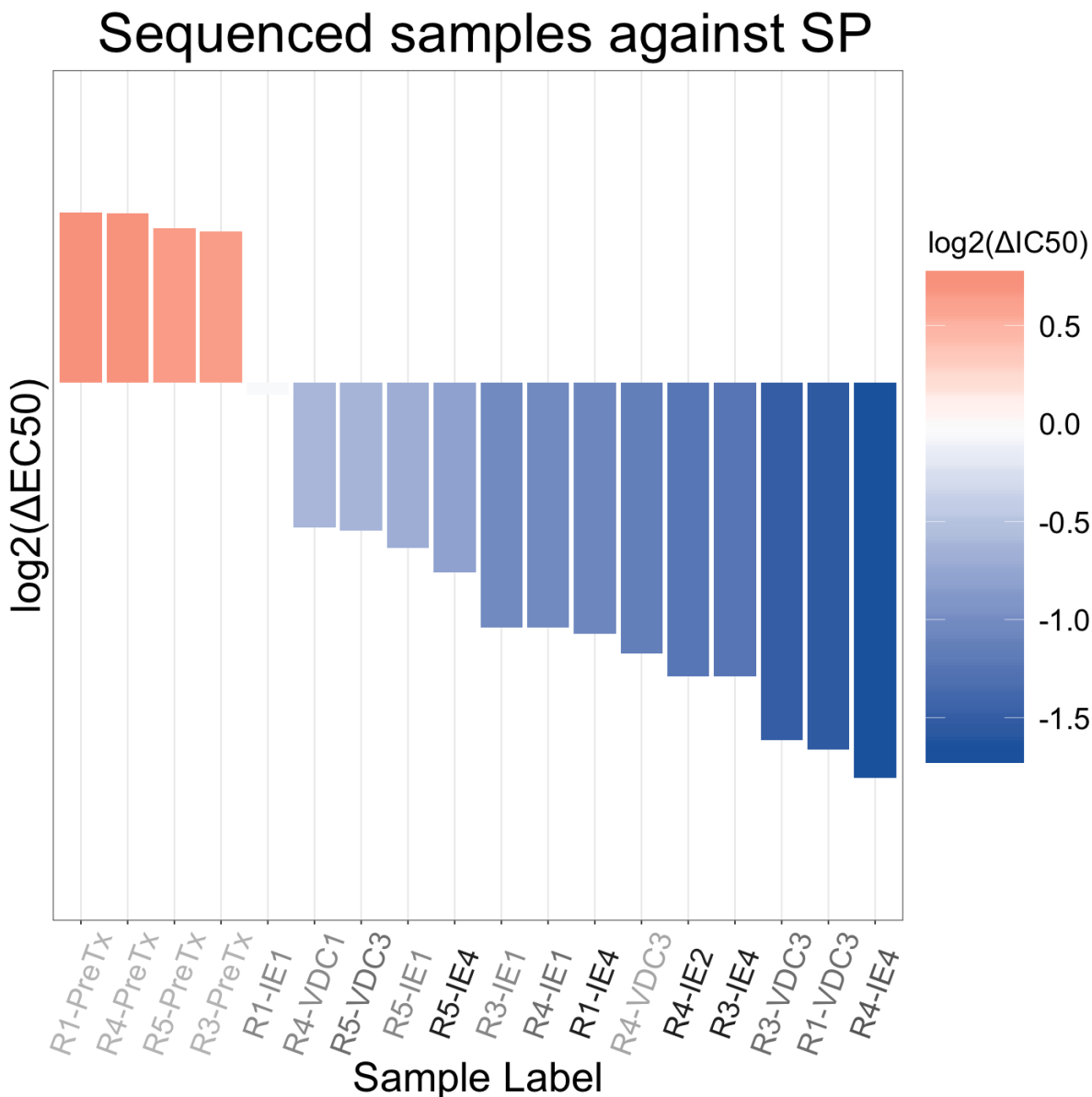
Sequenced samples against SAHA



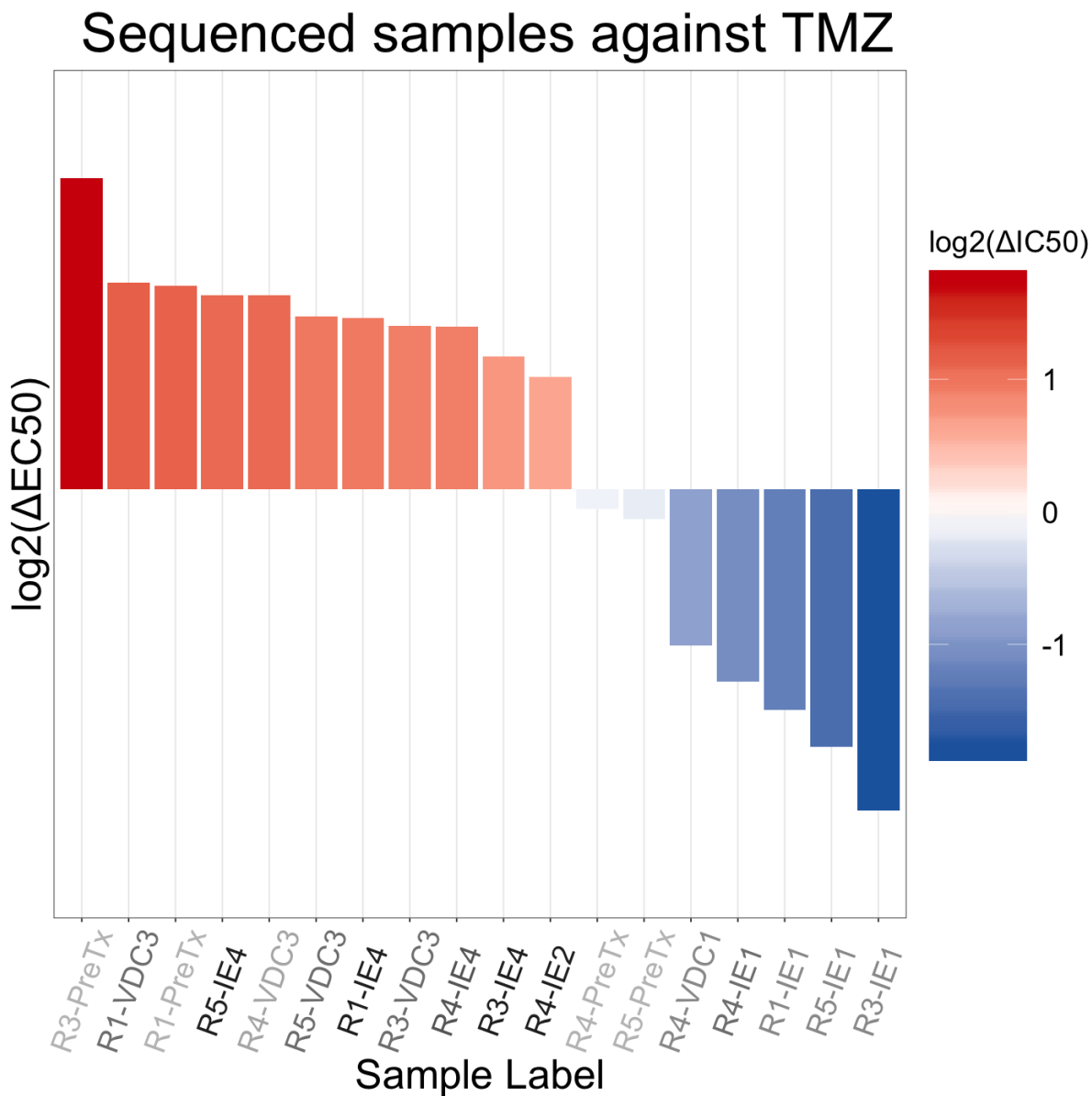
Supplementary Figure 12. Waterfall of EC₅₀ values for sequenced samples against vorinostat (SAHA). Color represents log₂ change in EC₅₀ between the sample and average control EC₅₀ at the given time point. Red shows a change towards resistance, while blue shows a change towards sensitivity. Samples are ranked along the x-axis from least-to-most sensitive. Sample labels on the x-axis are represented by darker colors the longer they have been evolved in the evolutionary experiment.



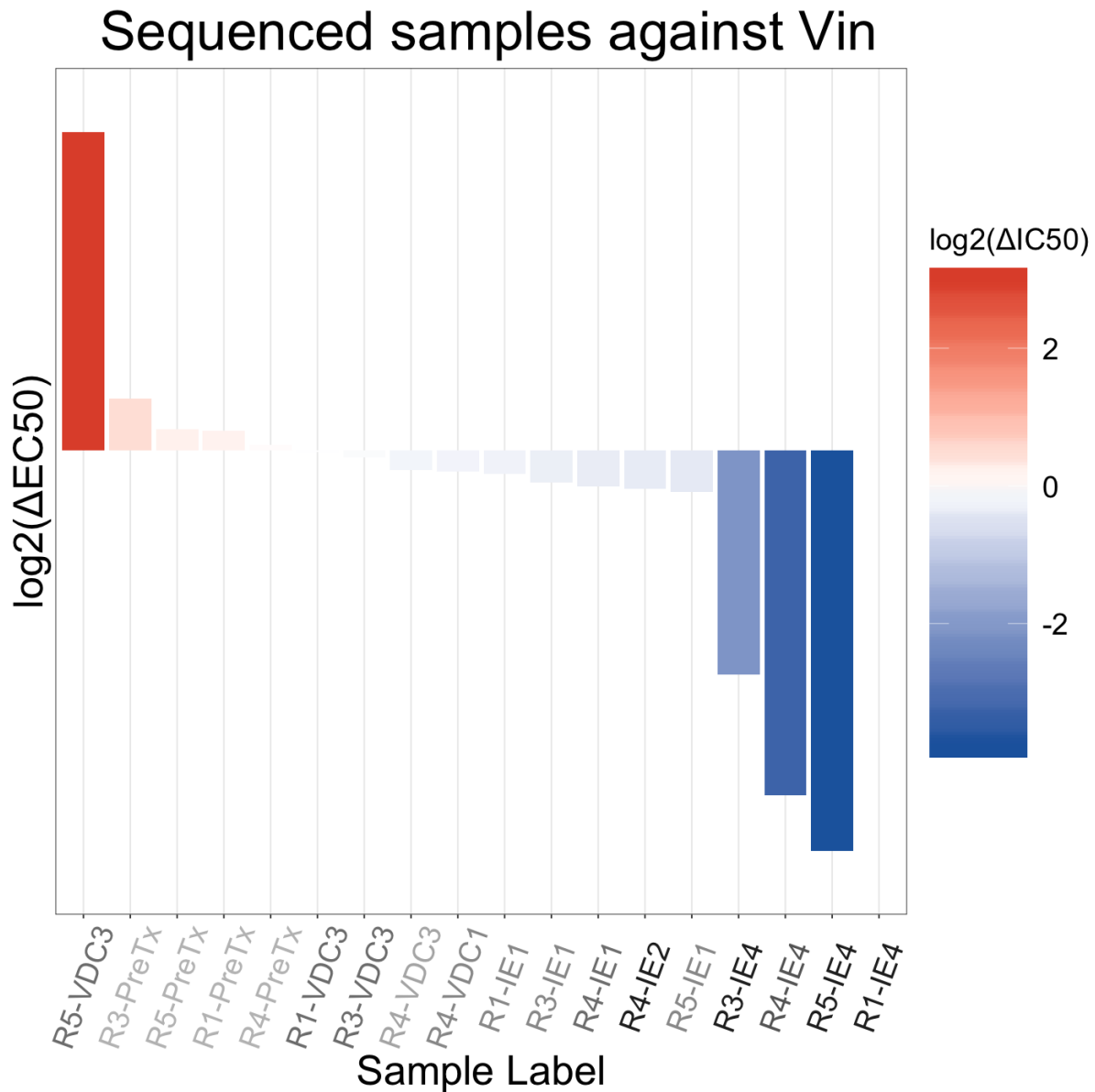
Supplementary Figure 13. Waterfall of EC₅₀ values for sequenced samples against irinotecan (active metabolite, SN38). Color represents \log_2 change in EC₅₀ between the sample and average control EC₅₀ at the given time point. Red shows a change towards resistance, while blue shows a change towards sensitivity. Samples are ranked along the x-axis from least-to-most sensitive. Sample labels on the x-axis are represented by darker colors the longer they have been evolved in the evolutionary experiment.



Supplementary Figure 14. Waterfall of EC₅₀ values for sequenced samples against SP-2509. Color represents \log_2 change in EC₅₀ between the sample and average control EC₅₀ at the given time point. Red shows a change towards resistance, while blue shows a change towards sensitivity. Samples are ranked along the x-axis from least-to-most sensitive. Sample labels on the x-axis are represented by darker colors the longer they have been evolved in the evolutionary experiment.



Supplementary Figure 15. Waterfall of EC50 values for sequenced samples against temozolomide. Color represents \log_2 change in EC50 between the sample and average control EC50 at the given time point. Red shows a change towards resistance, while blue shows a change towards sensitivity. Samples are ranked along the x-axis from least-to-most sensitive. Sample labels on the x-axis are represented by darker colors the longer they have been evolved in the evolutionary experiment.



Supplementary Figure 16. Waterfall of EC₅₀ values for sequenced samples against vincristine. Color represents \log_2 change in EC₅₀ between the sample and average control EC₅₀ at the given time point. Red shows a change towards resistance, while blue shows a change towards sensitivity. Samples are ranked along the x-axis from least-to-most sensitive. Sample labels on the x-axis are represented by darker colors the longer they have been evolved in the evolutionary experiment. The EC₅₀ for the first replicate after the fourth exposure to the EC drug combination (R1-IE4) was indeterminate and removed from the waterfall plot.